DYNAMICS OF WALL BOUNDED TURBULENCE

A THESIS SUBMITTED TO
THE GRADUATE SCHOOL OF NATURAL AND APPLIED SCIENCES
OF
MIDDLE EAST TECHNICAL UNIVERSITY

BY

OZAN TUĞLUK

IN PARTIAL FULFILMENT OF THE REQUIREMENTS
FOR
THE DEGREE OF MASTER OF SCIENCE
IN
ENGINEERING SCIENCES

FEBRUARY 2005

Approval of the Graduate School of Natural and Applied Sciences.

Prof. Dr. Canan Özgen
Director

I certify that this thesis satisfies all the requirements as a thesis for the degree of Master of Science.

Prof. Dr. Ruşen Gecit
Head of Department

This is to certify that we have read this thesis and that in our opinion it is fully adequate, in scope and quality, as a thesis for the degree of Master of Science.

Assoc. Prof. Dr. Hakan I. Tarman
Supervisor

Examining Committee Members

Prof. Dr. Cevdet Akgöz (METU, ES) _____

Assoc. Prof. Dr. Hakan I. Tarman (METU, ES) _____

Prof. Dr. Hasan Taşeli (METU, MATH) _____

Prof. Dr. Turgut Tokdemir (METU, ES) _____

Assist. Prof. Dr. Utku Kanoğlu (METU, ES) _____

I hereby declare that all information in this document has been obtained and presented in accordance with academic rules and ethical conduct. I also declare that, as required by these rules and conduct, I have fully cited and referenced all material and results that are not original to this work.

Name, Last Name : Ozan Tuğluk

Signature :

ABSTRACT

DYNAMICS OF WALL BOUNDED TURBULENCE

Ozan Tuğluk

M.S., Department of Engineering Sciences

Supervisor: Assoc. Prof. Dr. Hakan I. Tarman

February 2005, 77 pages

Karhunen-Loève decomposition is a well established tool, in areas such as signal processing, data compression and low-dimensional modeling. In computational fluid mechanics (CFD) too, KL decomposition can be used to achieve reduced storage requirements, or construction of relatively low-dimensional models. These relatively low-dimensional models, can be used to investigate the dynamics of the flow field in a qualitative manner. Employment of these reduced models is beneficial, as the they can be studied with even stringent computing resources. In addition, these models enable the identification and investigation of interactions between flowlets of different nature (the flow field is decomposed into these flowlets). However, one should not forget that, the reduced models do not necessarily capture the entire dynamics of the original flow, especially in the case of turbulent flows.

In the presented study, a KL basis is used to construct reduced models of Navier-

Stokes equations in the case of wall-bounded turbulent flow, using Galerkin projection. The resulting nonlinear dynamical systems are then used to investigate the dynamics of transition to turbulence in plane Poiseuille flow in a qualitative fashion. The KL basis used, is extracted from a flow filed obtained from a direct numerical simulation of plane Poiseuille flow.

Keywords: Wall bounded turbulence, Karhunen-Loève decomposition, Transition to turbulence, Galerkin projection

ÖZ

DUVAR SINIRLI TÜRBÜLANS DİNAMİĞİ

Ozan Tuğluk

Yüksek Lisans, Mühendislik Bilimleri Bölümü

Tez Yöneticisi: Doç. Dr. Hakan I. Tarman

Şubat 2005, 77 sayfa

Deneysel özdeğer fonksiyonlarına (Karhunen-Loève) ayrıştırma yöntemi, sinyal işleme, veri sıkıştırma, düşük boyutlu model oluşturma alanlarında kullanılan bir araçtır. Hesaplamalı akışkanlar mekaniğinde, bu yöntem benzer amaçlarla kullanılabilir. Bu alanda oluşturulan modeller, düşük hesaplama gücü gereksinimleri ve akış içerisindeki alt-akışların etkileşimlerinin incelenmesine olanak tanımalarından, yararlı olabilmektedir. Ancak bu indirgenmiş modellerin, özellikle türbülanslı akışlarda, akışın tüm dinamiğini kapsamayabileceği unutulmamalıdır.

Sunulan çalışmada, deneysel özdeğer fonksiyonları, Navier-Stokes denklemlerinin, duvar sınırlı türbülanslı akış özelinde, Galerkin projeksiyonu yöntemi ile, indirgenmiş modellerini oluşturmak için kullanılmıştır. Oluşturulan nonlineer dinamik sistemler, türbülansa geçiş bölgesinde akış dinamiğinin niteliksel incelenmesinde kullanılmıştır.

Anahtar Kelimeler: duvar sınırlı türbülans dinamiği, Deneysel özdeğer fonksiyonları, Türbülansa geçiş, Galerkin projeksiyonu

This work is dedicated to all the people whom it is not dedicated to ...

ACKNOWLEDGMENTS

I would like to thank my advisor, Hakan Tarman, first and foremost. His support, guidiance, enthusiasm was indespansible for this work. I would also like to thank him for keeping me focused during the course of my studies, without which this work would have never been completed.

I am grateful to my family for their continual support, encouragement, and friendship. I am indebted to my parents, Ali Rıza and Şadan, and my brother, Okan, for always being by my side.

I would like to thank Özlem for existing.

I cannot thank the Computer Center enough for employing me, which both enabled me to financially sustain myself and expand my knowledge. I also would like to thank CC for letting (even encouraging!) me to work on my thesis during the working hours. Thanks also go to all my co-workers, Ahmet Öztürk, Altay Özaygen, Burak Bilen, Çağlar Bilir, Cengiz Acartürk, Emre Sezginer, Feyza Eryol, Feride Erdal, Gökhan Eryol, Günce Çiftçi, Hasan Nadir Derin, İbrahim Çalışır, Selçuk Han Aydın, Suna Yılmaz, to name a few.

I want to express my gratitude for the peoples of baraka, and the household of DC59, for their friendship.

Last, but certainly not the least, the use of Debian GNU/Linux and a collection of free software, which exist thanks to the members of the free software community, which were indespensible for the presented work, is greatly acknowledged.

TABLE OF CONTENTS

LIST OF FIGURES

LIST OF TABLES

LIST OF ABBREVIATIONS

KL	: Karhunen-Loève
POD	: Proper Orthogonal Decomposition
EOF	: Empirical Orthogonal Function
EEF	: Empirical Eigenfunction
NS	: Navier Stokes
ODE	: Ordinary Differential Equation
3D	: Three Dimensional
$(\cdot)^*$	: Normalized $(\cdot)$ in friction units
$(\cdot)^+$	: Normalized $(\cdot)$ in wall units

CHAPTER 1

INTRODUCTION

Heisenberg is said to have said on his deathbed that, he would ask God two questions: why relativity and why turbulence?. Reportedly he added , "I really think he may have an answer to the first question."

To give a brief description, turbulence is a complex phonemena involving 3D, unsteady, nonlinear vortex activity on a large number of length and time scales. What makes turbulence rather unique is the fact that, almost all the simplifications/assumptions which make up theoretical fluid dynamics are invalid for turbulence. For example one cannot linearize NS equations to get turbulent solutions, turbulence is essentialy nonlinear. One cannot assume the turbulent flow is irotational unlike many problems in fluid mechanics. Also one cannot reduce the spatial dimension to 2 to simplify the solution (if one does, one simply destroys the problem). So it is not suprising that turbulence is a good object for scientific curiosity.

To sum up turbulence is a

- nonlinear
- highly unsteady
- dissipative (kinetic energy is transformed into internal energy)
- diffusive
- rotational
- 3D
- multiscale

phenomenon, which poses quite of an intellectual challenge to the researchers. In addition to the challanges involved, most flows in the universe are turbulent. In terms of engineering, turbulent flow means

- a large increase in drag
- a large decrease in momentum/flowrate
- cyclic structural loading, which causes fatigue
- increased noise
- increased/enhanced heat transfer
- increased/enhanced mixing

As can be deduced from the above list, prediction and *control* over turbulence is highly desirable on many occations. It is obvious that both prediction and *control* require a

fair understanding of underlying dynamics to be effective. This is why turbulence is an attractive area of study for the engineer.

We also should note that, virtually all flows are turbulent in nature, so one should not view turbulence as an exception, the real exception is the laminar flows. As noted earlier the common tools of theoretical fluid dynamics are inadequate for turbulent flows, so generally a *brute force* (i.e. numerical simulation) approach is employed, to gain insight to the underlying principles.

In the presented study, dynamics of turbulence, in the context of wall bounded turbulence, is studied through channel flow. Channel or plane Poiseuille flow (i.e. flow between two parallel plates and driven by uniform pressure gradient) is convenient for investigating the fundamental physics of wall bounded turbulence for a variety of reasons. One of the most important of these reasons is, unlike turbulent boundary layer over a flat plate which exhibits growth in streamwise direction, channel flow is homogeneous in spanwise and streamwise directions beyond the entrant flow region. Owing to this fact channel geometry is almost standard in experimental and numerical studies of wall-bounded turbulence.

In our work, we utilize a model consisting of a system of ODE's. The ODE's are obtained *á la Galerkin*, by projection of NS (*Navier-Stokes*) equations onto a space spanned by KL (*Karhunen-Loève*) modes. This simple idea is deeply rooted in dynamic systems theory and existence of characteristic large scale motions (coherent structures). A brief history is given below.

Owing to the processing power increase, first numerical simulations of turbulence were performed starting from 1970's (Deardorff, Orszag and Peterson, Schumann, Rogallo, Moin and Kim). As the ratio of (processing power)/(currency unit) increased,

the number of grid points and thus the resolution of the simulations improved significantly. This created a wealth of sufficeintly resolved turbulent flow field data available.

Meanwhile, the experimentalists came up with information, which implied the existince of underlying coherent structures in turbulent flows. [Cantwell, 1981] [1] The approaches to isolate coherent structures from the experimental observations varied from statistical correlation studies to flow visualization techniques.

On the theoretical front, the advances in dynamical systems theory and its applications to turbulence suggested such flows resided on relatively low dimensional attractors [Guckenheimer, 1986]. It was generally regarded that the underlying strange attractor could be characterized by the coordinates defined by the coherent structures. This idea is related to inertial manifolds, which manifest that long-term behaviour of an infinite dimensional system can be explained in terms of a small number of coordinates, provided the system has an inertial manifold.

At this point the KL expansion, which was suggested for use in turbulent flows by Lumley [Lumley, 1967, Lumley, 1970], was generally considered as the rational tool for extraction of the underlying coherent structures in turbulent flow. The well-resolved data needed for this procedure was available from the numerical simulations and from the experiments. The extraction of coherent structures, which were thought to roughly define the attractor for the flow, opened the scene for low dimensional models (for an excellent discussion consult [Sirovich, 1986]). The most famous (and perhaps the most controversial) of these models was the *Cornell model* [Aubry et al., 1988] which consisted of 5 complex equations (10 real), which was confined to the wall region and totally ignored longitidunal (streamwise) dependence in the flow.

[1] The presence of such structures was first discussed in mid 1950's [Townsend, 1956]

One of the oldest problems of fluid mechanics is the description of the mechanisms of growth of instabilities in laminar flows that lead to transition to turbulence. The behaviour of small-amplitude disturbances is reasonably well understood in contrast to finite-amplitude disturbances which is incomplete [Drazin and Reid, 1981]. There is yet no satisfactory agreement between theoretical and experimental studies of transition flows in general. This is especially true for the general class of shear flows for which wall-bounded flows and in particular plane Poiseuille or channel flow are examples.

The initial stages of transition in channel flow are theorized to start with the mean parabolic velocity profile loosing its stability to finite dimensional disturbances in a subcritical manner [Orszag and Kells, 1980, Orszag and Patera, 1983]. A new mathematical framework has been established recently to describe mechanisms of this subcritical bifurcation leading to secondary instability. This framework uses the tools like pseudospectra of nonnormal matrices to develop an algebraic theory of instability [Reddy and Trefethen, 1994, Trefethen, 1997]. Subsequent secondary instability analysis yields various scenarios of transition to turbulence involving streamwise vortices, oblique waves, streamwise streaks, and streak breakdown [Reddy et al., 1998, Schmid and Henningson, 2001].

The rest of this thesis is organized in five chapters. In Chapter 2, the general idea of KL decomposition procedure is presented. Chapter 3 will present the reader channel flow. Chapter 4 gives details about application of KL decomposition to channel flow. In Chapter 5, the reader may find the derivation of the model. Chapter 6 includes the results obtained together with conclusions drawn, the work is concluded with suggestions for future work.

CHAPTER 2

KL DECOMPOSITION

2.1 Karhunen-Loève decomposition

The idea behind KL decomposition/expansion is straightforward. Actually in science and engineering, a special case of KL-expansion, the Fourier series expansion, is frequently used. The KL expansion is the representation of a vector field $\mathbf{u}(\mathbf{x}, t)$ as a series of the form:

$$\mathbf{u} = \sum_{n=1}^{\infty} a_n(t)\, \boldsymbol{\phi}^{(n)}(\mathbf{x}) \tag{2.1}$$

in terms of an orthonormal set of functions $\boldsymbol{\phi}^{(n)}$,

$$(\boldsymbol{\phi}^{(n)}, \boldsymbol{\phi}^{(m)})_{\mathbf{x}} = \int_V \phi_j^{(n)} \phi_j^{(m)} dV = \delta_{nm} \quad \text{where} \quad j = 1, 2, 3 \tag{2.2}$$

summation convention on repeated indices, $(\cdot, \cdot)_{\mathbf{x}}$ denotes inner product over $\mathbf{x}$. The time dependent coefficients $\{a_n\}$ are also required to be statistically independent (sta-

tistically orthogonal),

$$E\{a_n a_m\} = \int a_n(t)\, a_m(t) dt = \lambda_n\, \delta_{nm} \tag{2.3}$$

Where $E\{\}$ indicates the ensemble average. As can be seen, the KL-decomposition decomposes the field $\mathbf{u}$ into space dependent (represented by a set of orthonormal functions, $\boldsymbol{\phi}^{(n)}$) and time dependent (represented by a_n) parts. The KL expansion is optimal in the sense that for any truncated representation,

$$\mathbf{u}^N = \sum_{n=1}^{N} a_n(t)\, \boldsymbol{\phi}^{(n)}(\mathbf{x}) \tag{2.4}$$

the sum:

$$E^N = \sum_{n=1}^{N} \lambda_n$$

is a maximum among similar representations. The physical importance of the above statement will be clarified in Chapter 4. The above requirements uniquely defining the KL-decomposition may seem exceedingly stringent, however, the orthonormal basis set $\{\boldsymbol{\phi}^{(n)}\}$ which are the eigenfunctions of the following integral equation:

$$\int_V K_{ij}(\mathbf{x}, \mathbf{x}')\, \phi_j^{(n)}(\mathbf{x}') dx' = \lambda_n \phi_i^{(n)}(\mathbf{x}) \tag{2.5}$$

whose kernel is the autocorrelation tensor of the field $\mathbf{u}$, i.e.

$$K_{ij}(\mathbf{x}, \mathbf{x}') = E\{u_i(\mathbf{x}, t), u_j(\mathbf{x}', t\})$$

satisfy the requirements stated above. Hence the KL-decomposition procedure man-

ifests itself as the solution of a integral eigenproblem. There are several methods for the solution of 2.5, these methods are presented briefly in Chapter 4. The fact that the kernel (autocorrelation tensor) in 2.5 is hermitian, non-negative and square integrable, assures that a uniformly convergent spectral representation for it exists (Mercer's Theorem [Riesz and Nagy, 1955]). So it is guaranteed that we have a complete set of orthonormal vector eigenfunctions $\boldsymbol{\phi}^{(n)}$ as solutions to 2.5. A more detailed discussion of the properties of the kernel can be found in [Sirovich, 1986].

KL decomposition (also called POD, EOF (*empirical orthogonal function*) analysis and EEF (*empirical eigenfunction*)), is used broadly in many disciplines. These include, but are not limited to, pattern recognition [Fukanaga, 1972] and geophysics [Preisendorfer, 1988], besides experimental and computational fluid mechanics.

2.2 Coherent structures

The concept of coherent structures in turbulent flow is rooted in the observation of organized structures in turbulent flow [Cantwell, 1981]. These observations naturally caused attempts to extract information on these structures from a given turbulent flow field.

However, until a theoretical framework supplied (see for example [Lumley, 1967]), such attempts generally lacked an objective definition of the so-called coherent structures. What this definition states is that, if such a structure exists it should be maximally correlated with the given turbulent flow field. In more mathematical terms, a coherent structure represented by a deterministic function $\phi_i(\cdot)$ should be as "nearly" parallel to a given ensemble of vector fields $u_i(\cdot)$ as possible in Hilbert space.

For a somewhat more detailed derivation for the structure and properties of the

eigenfunctions see Appendix A. In the preceeding statement $(\cdot)$ indicates dependence on a point in the chosen space. This leads to an equation for the coherent structures, ϕ_i), [Lumley, 1970].

$$\int R_{ij}(\cdot, \cdot')\, \phi_i(\cdot')\, d(\cdot') = \lambda \phi_i\,(\cdot) \tag{2.6}$$

where R_{ij} is two-point correlation function defined as

$$R_{ij}(\cdot, \cdot') = E\{u_i(\cdot) u_j(\cdot')\} \tag{2.7}$$

Here, R_{ij} regarded as a kernel is square integrable, non-negative, and hermitian. As a result, a complete set of orthonormal vector eigenfunctions as solutions to 2.6 is assured. So the random vector field representing a turbulent flow field, u_i, may be expanded in the coherent function basis as,

$$u(\cdot) = \sum_n a_n\, \phi_i^{(n)}(\cdot) \quad n = 1, 2, \cdots \tag{2.8}$$

$$a_n = \int u_i(\cdot) \phi_i^n(\cdot)\, d(\cdot) \tag{2.9}$$

and the above series converges in a mean square sense. In [Lumley, 1970], it is assumed that the eigenfunctions are ordered so that, $\lambda^{(1)}$, the largest eigenvalue corresponds to $\phi_i^{(1)}$. It is worthwhile to note here that the eigenvalues $\lambda^{(n)}$ represent the average fraction of flow energy along the corresponding eigenfunction, ϕ_i^n. From these, it follows that the expansion in 2.8 is optimal in the sense that, the fraction of energy along ϕ_i^n decreases rapidly as summation index n increases.

At this point it is clear that the expansion derived for coherent structures is similar to the KL decomposition of the turbulent velocity field. The quest for extraction of structure from an ensemble of experimental data or numerical solutions led to the consideration of KL decomposition as a possible tool. In the beginning phases, the KL decomposition had been thought as a faithful representation of the coherent structures, but, the existence of an homogeneous direction in the physical space leads to empirical eigenfunctions which are simply the Fourier modes. As this does not seem to agree with the observation of localised coherent structures, this view has been abandoned.

2.3 Applications

In this section we briefly list fields of application for the KL expansion.

Data compression: By employing KL compression one can achive a significant decrease in storage requirements for almost any data. We will focus on scientific computing, specifically CFD. Suppose a CFD calculation is performed on a $m \times n \times q$ grid, the storage required to store the flow field is (per time step) $3 \times m \times n \times q$ units. If we consider a rather coarse turbulence simulation on a $24 \times 48 \times 129$ grid for 5000 timesteps [1], the storage requirement is approximately 16.6 Gb per simulation. If KL decomposition is performed however, generally retaining the first few thousand modes is enough (i.e. first few thousand modes generally retain a large fraction of the total energy). If we suppose the first 5000 time dependent coefficients need to be stored ($a_n(t)$), the total storage requirment drops to about 190 Mb for each realization, plus a one time storage

[1] In an architecture where double precision numbers are represented with 8 bytes, like i386 for example

of library of KL eigenfunctions ($\boldsymbol{\phi}^{(n)}(\mathbf{x})$).[2] If we further assume data for 10 different conditions is stored, storing KL expansion coefficients with the library of KL eigenfunctions amounts to 10% of pointwise storage. The flow field can be recovered later by the expansion

$$\mathbf{u}^N = \sum_{n=1}^{N} a_n(t)\, \boldsymbol{\phi}^{(n)}(\mathbf{x})$$

Some examples of such wok can be found in data reduction in digital representation of human faces [Sirovich and Kirby, 1987], in experimental flow visualization of structures [Sirovich et al., 1990b] etc.

Low dimensional modeling: Suppose we have nonlinear differential equation given by

$$\frac{\partial u}{\partial t} = \mathcal{N}(u, \mathcal{R})$$

where $\mathcal{N}$ represents a nonlinear operator involving u, spatial derivatives of u, and parameters represented by $\mathcal{R}$. A low dimensional model capturing some important aspects of the equation may be constructed by projecting the original equation on a subspace spanned by the truncated KL expansion (i.e. via Galerkin projection). This can be done as follows: first the KL eigenfuncions are extracted from the field u, obtained by, say numerical simulation, at reference value $\mathcal{R}_o$. The expansion is substituted into the original equation,

$$\frac{d}{dt} \sum_{n=1}^{N} a_n\, \boldsymbol{\phi}^{(n)} = \mathcal{N}(\sum_{n=1}^{N} a_n\, \boldsymbol{\phi}^{(n)}, \mathcal{R})$$

[2] $5000 \times 24 \times 48 \times 129 \times 3$ bytes ($\approx$ 16 GB) for the eigenfunctions.

Performing the Galerkin procedure, results in an equation of the form

$$\frac{da_k}{dt} = \tilde{\mathcal{N}}(a_k, \mathcal{R}) \tag{2.10}$$

for the KL expansion coefficients a_k

This equation can be used to determine the time evolution of expansion coefficients and thus may constitute a low dimensional model for the original equation in the neighbourhood of $\mathcal{R}_o$. Note that optimality of the KL expansion is no longer available when used for off reference values of $\mathcal{R}$, however, the KL expansion functions $\boldsymbol{\phi}^{(n)}$ still satisfy all the spatial constraints on the field, such as boundary conditions, incompressibility conditions, etc. Some examples of such uses of KL expansion can be found in the studies of dynamics of Ginzburg-Landau equation [Sirovich et al., 1990c], transition in boundary layer flow [Sirovich and Zhou, 1994], transition in Rayleigh-Benard thermal convection flow [Tarman, 2003]].

CHAPTER 3

CHANNEL FLOW

3.1 Governing equations

Channel flow takes place in a physical domain, $-\infty < x, z < \infty;\ 0 < y < 2h$, and is driven by a uniform force k (pressure gradient) in the x-direction. Here x represents longitudional (streamwise), z lateral (spanwise), and y azimuthal (wall-normal/cross-channel) directions. The notation $\mathbf{u} = (u_1, u_2, u_3) = (u, v, w)$ will be used for flow velocities and $\mathbf{x} = (x_1, x_2, x_3) = (x, y, z)$ for the spatial coordinates interchangeably.

The boundary conditions are (imposed by the finite viscosity of the fluid, μ), the so-called no-slip boundary conditions,

$$\mathbf{u}(x, 0, z, t) = \mathbf{u}(x, 2h, z, t) = 0$$

Channel flow is ideal for the study of turbulence dynamics. In turbulent flows in channels the flow in longitudional (streamwise) and lateral (spanwise) directions is homogeneous (beyond the entrant flow region), contrast this with turbulent boundary layer where the boundary layer grows, albeit slowly, in the longitudional direction.

This property of the turbulent channel flow is a great simplification and thus made the channel the geometry of choice for experiments and numerical simulations alike.

If we accept that NS equations describe the turbulent flow adequately (for a brief discussion see [Holmes et al., 1998]), then the equations of motion are given by:

$$\frac{\partial u_j}{\partial x_j} = 0, \tag{3.1a}$$

$$\rho(\frac{\partial u_i}{\partial t} + \frac{\partial}{\partial x_j}u_i u_j) + \frac{\partial p}{\partial x_i} = k\delta_{i1} + \mu\nabla^2 u_i, \tag{3.1b}$$

and the boundary conditions are

$$u_i(x, 0, z, t) = u_i(x, 2h, z, t) = 0$$

for i, j=1,2,3.

The mean flow is, $\langle u_i \rangle = U(y)\delta_{i1}$, given by

$$\langle u_i \rangle \equiv \lim_{T\to\infty} \frac{1}{T} \int_{-T/2}^{T/2} u_i(\mathbf{x}, t)dt \equiv \lim_{A\to\infty} \frac{1}{T} \int_A u_i(\mathbf{x}, t)dxdz$$

where A denotes the area of the x-z plane of the channel. The last equivalence follows from the assumption of ergodicity which states that time averaging is equivalent to spatial averaging over homogeneous directions, provided that A and T are sufficiently large. If the flow is decomposed into the components of the mean and the fluctuations from the mean by

$$\mathbf{u} = \langle \mathbf{u_i} \rangle + \mathbf{u}'$$

and substituted into the NS equations, deemed as governing equations (3.1), it follows

that that $\mathbf{u}'$ satisfies:

$$\rho\left\{\frac{\partial u_i'}{\partial t}+\frac{\partial}{\partial x_j}u_i'u_j'\right\}+\frac{\partial p'}{\partial x_i}=-\rho\left\{U\frac{\partial u'}{\partial x}+\delta_{i1}\left(v'\frac{\partial U}{\partial y}-\frac{\partial}{\partial y}\langle u'v'\rangle\right)\right\}+\mu\nabla^2 u_i' \quad (3.2)$$

and the mean flow satisfies

$$k=-\frac{\partial}{\partial y}\left\{\mu\frac{\partial U}{\partial y}-\rho\langle u'v'\rangle\right\}. \quad (3.3)$$

It should be noted that the fluctuating component is driven by the interactions with the mean flow, in contrast to the mean flow component which is driven by the constant uniform pressure gradient k. From now on the primes on the velocity shall be dropped and unless otherwise explicitly stated, $\mathbf{u}$ will signify the fluctuation velocities. (3.3) states that the uniform pressure gradient k is balanced by the Reynolds stress $(-\rho\langle u'v'\rangle)$ and by the shear stress due to mean flow$(\mu\frac{\partial U}{\partial y})$, which can be interpreted as the pressure force being balanced by microscopic and macroscopic transport of momentum to the walls. The equation for the mean can be integrated twice to yield

$$U(y)=\frac{1}{\nu}\int_0^y\langle u'v'\rangle dy\ +\frac{u_\tau^2}{\nu}\left(\frac{2hy-y^2}{2h}\right).$$

In the absence of turbulence (i.e. in the case laminar flow), the above equation is reduced to

$$U(y)=\frac{u_\tau^2}{\nu}\left(\frac{2hy-y^2}{2h}\right)$$

which is the well-known parabolic velocity profile.

The wall skin friction is, by a simple force balance,

$$\tau = \mu \frac{\partial U}{\partial y}|_{(y=0)} = kh,$$

and the friction velocity may be defined as:

$$u_\tau = \sqrt{\tau/\rho} = \sqrt{kh/\rho}.$$

And via the friction velocity a wall length scale can be defined through

$$l_\tau = \frac{\nu}{u_\tau}.$$

While l_τ and u_τ are reffered to as the micro scales, the channel half height, h, and the centerline velocity, U_{CL}, are called as macro scales and scale the core region. Another macroscale for the velocity is the so-called bulk velocity,

$$U_b = \frac{1}{2h} \int_0^{2h} U(y)\, dy.$$

Nondimensionalization (normalization) provided by the scales, u_τ for velocity; h for length; h/u_τ for time, i.e.:

$$\frac{\mathbf{u}}{u_\tau} \rightarrow \mathbf{u}^*; \;\; \frac{\mathbf{x}}{h} \rightarrow \mathbf{x}^*; \;\; \frac{t}{h/u_\tau} \rightarrow t^*; \;\; \frac{p}{\rho u_\tau^2} \rightarrow p^*,$$

leads to normalized form of NS equations:

$$\frac{\partial u_j^*}{\partial x_j^*} = 0, \tag{3.4a}$$

$$\frac{\partial u_i^*}{\partial t^*} + \frac{\partial}{\partial x_j^*} u_i^* u_j^* + \frac{\partial p^*}{\partial x_i^*} = \delta_{i1} + \frac{1}{R_\tau} \nabla^2 u_i^*, \tag{3.4b}$$

with Reynolds number given by:

$$R_\tau = \frac{u_\tau h}{\nu} = \frac{h}{l_\tau}.$$

Another normalization is possible, with l_τ for the length scale. The resulting units after this normalization are called *wall units*. This normalization is given by:

$$\frac{\mathbf{u}}{u_\tau} \to \mathbf{u}^+; \ \frac{\mathbf{x}}{l_\tau} \to \mathbf{x}^+; \ \frac{t}{h/u_\tau} \to t^+.$$

The conversion between friction and wall units:

$$y^+ = \frac{y}{l_\tau} = \frac{y R_\tau}{h} = y^* R_\tau,$$

$$t^+ = t^* R_\tau.$$

The wall units measure smaller scales in the near wall region and commonly called the micro units. The friction units are sometimes referred to as macro units. The next section gives a somewhat more detailed discussion of the nondimensionalizations.

3.2 Scales and normalizations

In this section, some details and justifications about the nondimensional units utilized are given with asymptotic analysis of the resulting nondimensional equations.

Consider (3.3), this equation when integrated once yields:

$$-\frac{ky}{\rho} = -\langle u'v' \rangle + \nu \frac{dU}{dy} - u_\tau^2 \tag{3.5}$$

Where u_τ is the friction velocity defined in the previous section and is related to the gradient of the mean flow at the wall. If the friction velocity is written in open form ($u_\tau = \sqrt{kh/\rho}$) in (3.5), we get

$$u_\tau^2 \left(1 - \frac{y}{h}\right) = -\langle u'v' \rangle + \nu \frac{dU}{dy}. \tag{3.6}$$

If (3.6) is nondimensionalized by u_τ and h

$$1 - \frac{y}{h} = -\frac{\langle u'v' \rangle}{u_\tau^2} + \frac{\nu}{u_\tau h} \frac{d(U/u_\tau)}{d(y/h).} \tag{3.7a}$$

Employing the nondimensional frictional units yields,

$$1 - y^* = -\frac{\langle u'v' \rangle}{u_\tau^2} + \frac{1}{R_\tau} \frac{du^*}{dy^*} \tag{3.7b}$$

It is vital to note, that for large values of the friction Reynolds number ($R_\tau = u_\tau h/\nu$), the viscous stress is supressed by this nondimensional form. As the stress at the wall is predominantly viscous in nature, this normalization cannot be valid near the wall as $R_\tau \to \infty$. This is why the second unit system (*wall units*) was presented in the

preceeding section.

So one needs to define another unit system (i.e. nondimensional form), in the immediate vicinity of the wall so that the viscous term does not diminish for large values of R_τ. One way to achive this, is to simply absorb the friction Reynolds number in the length scale. With this modification (3.6) becomes,

$$1 - \frac{y}{h} = -\frac{\langle u'v' \rangle}{u_\tau^2} + \frac{d(U/u_\tau)}{d(yu_\tau/\nu).} \tag{3.8a}$$

Employing the nondimensional wall units yields,

$$1 - \frac{y^+}{R_\tau} = -\frac{\langle u'v' \rangle}{u_\tau^2} + \frac{du^+}{dy^+.} \tag{3.8b}$$

Clearly the form stated in (3.8b) tends to supress the change of stress in the y-direction as $R_\tau \to \infty$. Now let us investigate (3.7b, 3.8b) asymptotically as $R_\tau \to \infty$.

Provided that y^* remains $\mathcal{O}(1)$, (3.7b) reduces to

$$1 - y^* = -\frac{\langle u'v' \rangle}{u_\tau^2} \tag{3.9}$$

This equation cannot be valid as $y^* \to 0$, which corresponds to finite values of y^+ (i.e. the vicinity of the wall). The part of the flow where (3.9) holds, is called the **core region**.

(3.8b), can be written as, y^+ being $\mathcal{O}(1)$,

$$1 = -\frac{\langle u'v' \rangle}{u_\tau^2} + \frac{du^+}{dy^+} \tag{3.10}$$

The above equation is not valid as $y^+ \to \infty$ (the core region). The region of validity

for (3.10) is called as the **surface layer**.

The two layer description (surface layer - core region) presented above requires a matching region. This matching should be done in a region characterized by the limits $y_+ \to \infty$ and $y^* \to 0$. This can be achived by a process known as aymptotic matching [Tennekes and Lumley, 1972]. This overlap region is a region of approximately constant Reynolds stress. The viscous stress on the other hand is very small compared to Reynolds stress in this region. Due to this lack of local viscous effects, this overlap region is called **inertial sublayer**. Since the stress at the surface is purely viscous in nature, as one moves down the inertial sublayer towards the wall there should be a region in which viscous stresses dominate over Reynolds stresses (this is also suggested by experimental evidence). This region is called the **viscous sublayer** and extends up to about $y^+ = 5$. The region where the viscous and inertial sublayers merge is called the **buffer layer**. In this region neither of the two stress components can be ignored. This layer is also the site for maximum turbulent energy production, which occurs approximately at $y^+ = 12$.

3.3 Kinetic Energy of Turbulence

The equations of motion for steady mean flow in an uncompressible fluid are

$$\frac{\partial U_i}{\partial x_i} = 0, \quad U_j \frac{\partial U_i}{\partial x_j} = \frac{\partial}{\partial x_j}\left(\frac{T_{ij}}{\rho}\right), \tag{3.11}$$

where T_{ij} is defined by $T_{ij} = -P\delta_{ij} + 2\mu S_{ij} - \rho\langle u_i' u_j' \rangle$. The mean rate of strain S_{ij} is defined as

$$S_{ij} = \frac{1}{2}\left(\frac{\partial U_i}{\partial x_j} + \frac{\partial U_j}{\partial x_i}\right).$$

The equation governing the dynamics of the mean flow kinetic energy ($\frac{1}{2}U_iU_i$) is obtained by multiplying (3.11)

$$\rho U_j \frac{\partial}{\partial x_j}\left(\frac{1}{2}U_iU_i\right) = \frac{\partial}{\partial x_j}\left(T_{ij}U_{ij}\right) - T_{ij}\frac{\partial U_i}{\partial x_j} = \frac{\partial x_j}{(T_{ij}U_{ij})} - T_{ij}S_{ij}. \tag{3.12}$$

Here, the first term on the right-hand side represents transport of mean-flow energy by the stress T_{ij}, which integrates to zero over the control volume on whose surfaces either T_{ij} or U_i vanishes. The term $T_{ij}S_{ij}$ is called deformation work which represents kinetic energy of the mean flow that is lost to or retrived from the agency that generates the stress. After substituting the stress tensor expression, we have

$$-T_{ij}S_{ij} = -2\mu S_{ij}S_{ij} + \rho\langle u_i'u_j'\rangle S_{ij}$$

The term $2\mu S_{ij}S_{ij}$ is called viscous dissipation.

The equation governing the mean kinetic energy $\frac{1}{2}\langle u_i'u_i'\rangle$ of the turbulent velocity fluctuations is obtained by $u_i = U_i + u_i'$, taking the time average of all terms and subtractiong (3.12) one gets

$$\rho U_j \frac{\partial}{\partial x_j}\left(\frac{1}{2}\langle u_i'u_i'\rangle\right) = -\frac{\partial}{\partial x_j}\left(\langle u_j'p\rangle + \frac{1}{2}\langle u_i'u_i'u_j'\rangle - 2\mu\langle s_{ij}s_{ij}\rangle - \rho\langle u_i'u_j'\rangle S_{ij}\right), \tag{3.13}$$

where the quantity s_{ij} is the fluctuating rate of strain given by

$$s_{ij} = \frac{1}{2}\left(\frac{\partial u_i'}{\partial x_j} + \frac{\partial u_j'}{\partial x_i}\right).$$

The divergence (transport) terms on the right-hand side merely redistribute energy from one point in the flow to another, if the energy flux out of or into a closed volume is zero.

The term $\rho\langle u_i' u_j'\rangle S_{ij}$ occurs in (3.12) and in eqn. (3.13) with opposite signs. Since normally negative values of $\langle u_i' u_j'\rangle$ tend to occur in situations with positive S_{ij}, this term apparently serves to exchange kinetic energy between the mean flow and turbulence. Normally, the energy exchange involves a loss to the mean flow and a gain to turbulence[1]. Thus this term is called turbulent energy production.

3.4 Energy Flow between Layers

In the particular case of channel flow, $U_i = U(y)\delta_{i1}$, the mean flow kinetic energy reads

$$kU = -\frac{d}{dy}\left(U\left\{\mu\frac{dU}{dy} - \langle u'v'\rangle\right\}\right) + \mu\left(\frac{dU}{dy}\right)^2 - \rho\langle u'v'\rangle\frac{dU}{dy}.$$

The surface layer is a sink for momentum and therefore also for kinetic energy associated with the mean flow. Mean flow kinetic energy transferred into the surface layer by Reynolds stresses $d(\langle u'v'\rangle U)/dy$ is converted into turbulent kinetic energy $\langle u'v'\rangle(dU/dy)$ (turbulence production) and into heat $\nu(dU/dy)^2$ (viscous dissipation). If we integrate the transport term, $d(\langle u'v'\rangle U)/dy$, over the control volume covering the surface layer, we obtain an energy input to the surface layer of order $\rho U {u_\tau}^2$ per unit area and time, because U is fairly close to U_{CL} at the edge of the surface layer. The direct loss of order $\rho {u_\tau}^3$ to viscous dissipation occurs primarily in the viscous sublayer of ν/u_τ thickness within the surface layer. Most of the mean flow energy transported into the surface layer is thus used for maintanance of turbulent kinetic energy. In

[1] This has been recently disputed in [Jiménez and Simens, 2000]

the core region, on the other hand, the Reynolds stress is of order ρu_τ^2 and dU/dY is of order u_τ/h. Integrating over the entire core region, the turbulence production per unit area and time in the core region is of order $\rho {u_\tau}^3$. So it seems plausible to conclude that, most of the turbulence production occurs in the surface layer, while the rate of dissipation of turbulent energy is also high there. The main function of the core region is thus transport of mean flow kinetic energy into the surface layer, where it is converted into turbulent kinetic energy.

3.5 Linear Stability

Consider the linearized form of the governing equations for the fluctuations from the mean (3.2),

$$\frac{\partial u}{\partial t} + U\frac{\partial u}{\partial x} + vU' = -\frac{\partial p}{\partial x} + \frac{1}{Re}\nabla^2 u, \tag{3.14a}$$

$$\frac{\partial v}{\partial t} + U\frac{\partial v}{\partial x} = -\frac{\partial p}{\partial y} + \frac{1}{Re}\nabla^2 v, \tag{3.14b}$$

$$\frac{\partial w}{\partial t} + U\frac{\partial w}{\partial x} = -\frac{\partial p}{\partial z} + \frac{1}{Re}\nabla^2 w, \tag{3.14c}$$

where the primes on the fluctuating components are dropped and $(')$ denotes a y-derivative. Here we followed the convention and used a scaling based on the centerline velocity U_{CL}, thus $Re = U_{CL}h/\nu$. The above set of equations is completed by the continuity equation

$$\frac{\partial u}{\partial x} + \frac{\partial v}{\partial x} + \frac{\partial w}{\partial x} = 0. \tag{3.15}$$

Taking the divergence of the linearized momentum equations (3.14) and using the continuity equation (3.15) yields an equation for the fluctuation pressure:

$$\nabla^2 p = 2U' \frac{\partial v}{\partial x},$$

This equation may be used with the second equation (3.14) to eliminate p, resulting in an equation for the normal velocity, v:

$$\left[\left(\frac{\partial}{\partial t} + U \frac{\partial}{\partial x} \right) \nabla^2 - U'' \frac{\partial}{\partial x} - \frac{1}{Re} \nabla^4 \right] v = 0. \tag{3.16}$$

In order to complete the description of the flow field, a second equation is obtained for the normal vorticity,

$$\eta = \frac{\partial u}{\partial z} - \frac{\partial w}{\partial x},$$

where it satisfies

$$\left[\frac{\partial}{\partial t} + U \frac{\partial}{\partial x} - \frac{1}{Re} \nabla^2 \right] \eta = -U \frac{\partial v}{\partial x}. \tag{3.17}$$

The pair of equations (3.16) and (3.17) are considered with the boundary conditions

$$v = v' = \eta = 0,$$

at the walls.

Next, wave like solutions are introduced of the form

$$v(x,y,z,t) = \hat{v}(y)e^{i(\alpha x+\beta y-\omega t)},$$

$$\eta(x,y,z,t) = \hat{\eta}(y)e^{i(\alpha x+\beta y-\omega t)},$$

where α and β denote the streamwise and spanwise wave numbers respectively, and ω stands for the frequency. Introducing this representation into (3.16) and (3.17) results in the following pair of quations for $\hat{v}$ and $\hat{\eta}$

$$\left[(-i\omega + i\alpha U)(D^2 - k^2) - i\alpha U^* - \frac{1}{Re}(D^2 - k^2)^2\right]\hat{v} = 0, \tag{3.18}$$

$$\left[(-i\omega + i\alpha U) - \frac{1}{Re}(D^2 - k^2)\right]\hat{\eta} = -i\beta U'\hat{v}, \tag{3.19}$$

with the boundary conditions $\hat{v} = D\hat{w} = \hat{\eta} = 0$ at the walls. Here D stands for differentiation operator in the normal (y) direction and $k^2 = \alpha^2 + \beta^2$. These are the classical Orr-Sommerfeld and Squire equations [Drazin and Reid, 1981, Schmid and Henningson, 2001]. The frequency ω appears as the eigenvalue in the Orr-Sommerfeld equation, together with the associated eigenfunctions $\hat{v}$ is generally complex. The spatial wave numbers α and β are assumed to be real.

The critical Reynolds number for the Orr-Sommerfeld equations is computed by Orszag as $Re_c = 5777.22$ [Orszag, 1971] corresponding to $\alpha = 1.02055$ and $\beta = 0$, which is in line with Squires theorem;

Squire's Theorem. *If a three dimensional mode is unstable, a two-dimensional mode* ($\beta = 0$) *is unstable at a lower Reynolds number.*

The Orr-Sommerfeld eigenproblem is solved by a Matlab routine (see Appendix

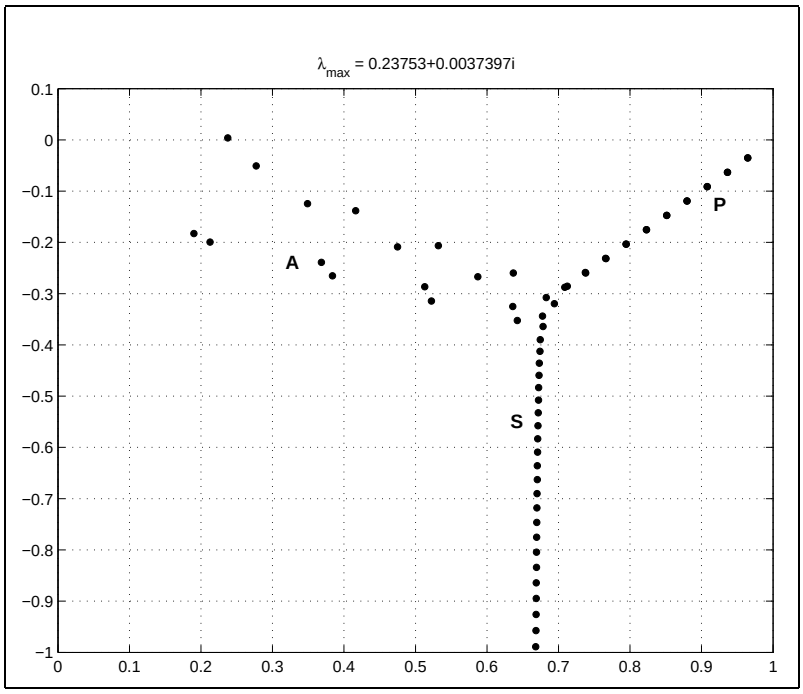

Figure 3.1: Spectrum of Orr-Sommerfeld equation, Re=10000, $\alpha = \beta = 1$.

B) resulting in the typical Y-shaped spectrum figure 3.1 for Re=10000 and wave numbers $\alpha = 1$ and $\beta = 0$. In this case, there is one slightly unstable mode on the branch A, which is called a Tollmien-Schlichting wave. This is remarkable in that the Orr-Sommerfeld equation has unstable disturbances for flows without inflection points. According to Rayleigh's inflection point criterion of inviscid linear stability theory:

Inflection Point Criterion. *If there exist perturbations with* $c_i > 0$*, then* $U''(y)$ *must vanish for some* $y \in [-1, 1]$.

the Poiseuille profile is stable as $Re \to \infty$, thus viscosity in this case is destabilizing.

The eigenvalues in (3.1) are located on three main branches which have been labeled A ($c_r \to 0$), P ($c_r \to 1$), and S ($c_r \approx 2/3$) where $\omega = c_r + ic_i$. The typical shapes of the corresponding eigenfunctions are shown in figure 3.2. Downwards in the

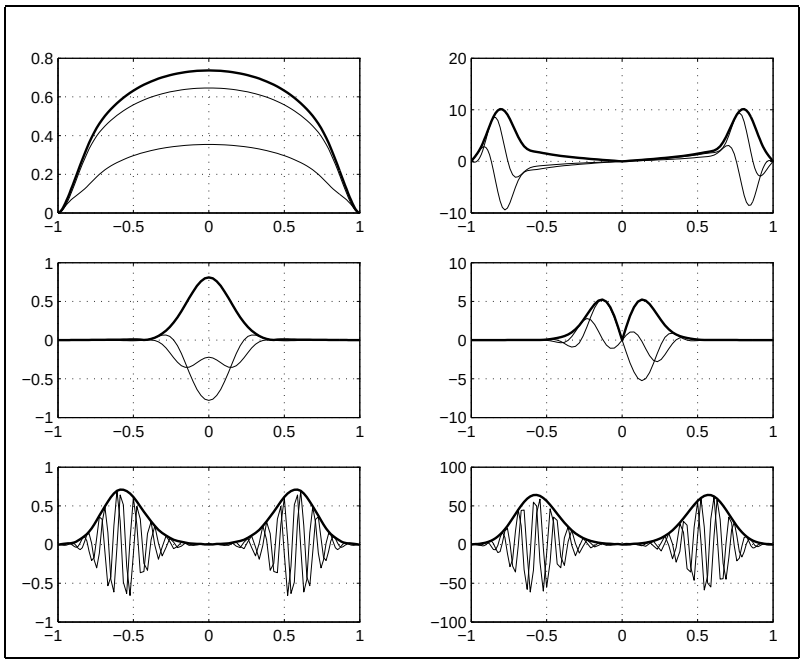

Figure 3.2: Eigenfunctions of Orr-Sommerfeld equation, Re=5000, $\alpha = \beta = 1$ left normal velocity, right normal vorticity.

S-branch, the wave length λ of the disturbance becomes shorter, so viscosity dominates via $\nu\nabla^2 u \approx -\nu\lambda^{-2}u$. The two branches (A and P) show the influence of the advection $(U \cdot \nabla u) + (u \cdot \nabla)U$ in the equation of motion. If u is localized near the wall, it moves very slowly downstream, and thus ($c_r \to 0$). It is apperent from the shape of the A modes which have their largest variation close to the wall that they are designated as wall modes and have rather small phase velocities. If u is localised in the center, it moves with the U_{CL}, therefore ($c_r \to 1$). The P modes have their maxima close to the center of the channel and have much higher phase speeds. They are designated as center modes. The highly damped S modes move with a medium velocity, $c_r \approx 2/3$. As Re increased, the wall modes are hardly influenced, the center and the damped modes are faster. The merging point of the branches moves down and to the right.

CHAPTER 4

KL DECOMPOSITION APPLIED TO CHANNEL FLOW

s The application of any orthogonal decomposition precedure requires a complete sufficiently resolved data set to work on. Advances in integrated circuit technology has made direct numerical simulations feasible (DNS), DNS in turn made available data sets of entire flow fields. Currently however, the processing speed required for a direct simulation of turbulent flows in complex geometries or at very high flow velocities is not reached, this is why in practical engineering problems turbulence models or large eddy simulation (LES) techniques are employed. For an interesting "asymptotic" account of computational cost of turbulence simulations (LES and DNS) and the future of turbulence research consult [Jiménez, 2003].

As mentioned above, application of KL-decomposition to turbulent flow is generally[1] preceeded by a direct numerical simulation. After the 4 dimensional velocity field is computed, the KL procedure is used to extract KL modes (eigenfunctions).

[1] Generation of approximate KL modes is also possible by machine learning techniques.

The eigenfunctions obtained can then be utilized for further study.

4.1 Turbulence simulation

The DNS of turbulent channel flow is, generally, either conducted by a pseudospectral (spectral collocation) or a spectral element method. As the name implies in DNS, no assumptions regarding the physics of the flow are made, and all the scales are resolved (i.e. all the scales which can be represented by the selected basis are resolved without discrimination). In this section we present the DNS of turbulence via a pseudospectral scheme, as this is the method employed in generation of the utilized data set.

The equations to solve numerically are the nondimensional NS equations (3.4). The solution is obtained by a pseudospectral algorithm due to Kim, Moin and Moser [Kim et al., 1987]. In this algorithm the velocity field is approximated by a Fourier-Chebyshev expansion, given by

$$\mathbf{u}(\mathbf{x},t) = \sum_{m=-\frac{M}{2}}^{\frac{M}{2}-1} \sum_{n=-\frac{N}{2}}^{\frac{N}{2}-1} \sum_{p=0}^{P} a_{mnp}(t)\, T_p(x_2) e^{ik_1 x_1} e^{ik_3 x_3}, \tag{4.1}$$

where $T_p(x_2)$ denotes the Chebyshev polynomials, the complex exponentials are due to Fourier expansion, $k_1 = 2\pi m/L_1$, $k_3 = 2\pi n/L_3$. Where L_1 and L_3 are the domain lengths in the x_1 and x_3 directions respectively.

We used a data set generated by Webber *et al.* [Webber et al., 1997] in which $L_1 = \pi$, $L_3 = 0.3\pi$ and the resolution is $48 \times 129 \times 24$ in the longitudinal, wall-normal, and lateral directions, respectively. The friction Reynolds number for the simulation (R_τ) was set to 135.5.

Weber et al. performed the decomposition based on the numerical data obtained for a minimal channel. The minmal channel concept was devised by J. Jimenez and

P. Moin [Jiménez and Moin, 1990], and defined by them as the minimum size of the periodic computational box that would sustain turbulence. In their simulation, Weber et al., used a minimal channel which can be viewed as a $1/5^{th}$ lateral-slice of the original full channel. They defined the minimal channel to be the slice of the wide channel in which just one roll pair appears. The minimal channel is only a model of the full channel and can be inaccurate is some important dynamical aspects, and higher order turbulence statistics, however, as dimension is an extensive quantity, when only a lateral slice of $1/5$ spanwise length is considered, the attractor dimension also roughly drops by a factor of 5. In the light of these considerations, the minimal channel is a considerably simpler laboratory to be used in exploring the dynamics of wall turbulence.

Note that in the simulation $y^* \in [-1, 1]$, which is the canonical interval.[2]

4.2 The decomposition

In application of KL procedure to turbulent channel flow, the flow is generally separated into mean and fluctuating components

$$\mathbf{u}(x_1, x_2, x_3, t) = U(x_2)e_1 + \mathbf{u}'(x_1, x_2, x_3, t). \tag{4.2}$$

Before the extraction of the KL modes, where $U(x_2)$ is the mean flow as defined in Chapter 3, however this is not followed in the presented work. The KL mode extraction is performed on the full flow field. Henceforth the prime on u' will be dropped and unless otherwise explicitly stated u will denote the fluctuations from the mean.

The velocity field is homogenous in the x_1 and x_3 directions, so that the velocity

[2] So $y \in [-h, h]$

field is translationally invariant over the horizontal plane. It follows that a direct KL analysis is possible via Fourier transform of $\mathbf{u}$ in the x_1 and x_3 directions,

$$\mathbf{u}^{(k)}(\mathbf{x},t) = \sum_m \sum_n \hat{u}^{(k)}(m,n;\ x_2) e^{i(k_1 x_1 + k_3 x_3)}, \tag{4.3}$$

and averaging the correlation over the entire ensemble

$$\kappa_{ij}(m,n;\ x_2,x_2') = \frac{1}{K}\sum_{k=1}^{K} \hat{u}_i(m,n;\ x_2)\overline{\hat{u}}_j(m,n;\ x_2'),$$

where the overbar denotes the complex conjugation. So it follows that for each wave number pair (n,m) the empirical eigenfunctions ϕ, and eigenvalues λ are determined from

$$\int_{-h}^{h} \kappa_{ij}(m,n;\ x_2,x_2')\,\phi_j(m,n;\ x_2')\,dx_2' = \lambda(m,n)\phi_i(x_2) \tag{4.4}$$

with i, j=1, 2, 3. Here also note that κ is the discrete Fourier transform of two point spatial correlation tensor given in section 2.1.

Once the empirical eigenfunctions are calculated from eqn.(4.4), the KL modes are given by

$$\mathbf{\Psi^{(k)}}(x_1,x_3,x_2) = e^{(i\frac{2\pi m}{L_1}x_1)}\, e^{(i\frac{2\pi n}{L_3}x_3)}\, \mathbf{\Phi^{(k)}}(x_2), \tag{4.5}$$

where $\mathbf{k} = (m,n,q)$ and q is referred to as the vertical quantum number (often abbreviated as quantum number).

The velocity field then, can be expressed as

$$\mathbf{u}(\mathbf{x},t) = \sum_{\mathbf{k}} a_{\mathbf{k}}(t)\, \mathbf{\Psi^{(k)}}(\mathbf{x}), \tag{4.6}$$

where the KL-coefficients are obtained from the inner product

$$a_{\mathbf{k}}(t) = (\mathbf{u}, \overline{\mathbf{\Psi}}^{(\mathbf{k})})_\omega = \int_V \mathbf{u}(\mathbf{x}, t) \cdot \overline{\mathbf{\Psi}}^{(\mathbf{k})}(\mathbf{x}) \cdot \omega(\mathbf{x}) dV, \tag{4.7}$$

and $(\cdot, \cdot)_\omega$ denotes the weighted inner product with respect to weight ω. This weight is the weight with respect to which the *K-L* eigenfunctions are orthonormal, is borrowed from the orthogonality considerations of Chebyshev expansion polynomials, given by form as :

$$\omega_j = \frac{\pi}{N_y} \sin\left(\frac{\pi j}{N_y}\right) \qquad j = 0, \ldots, N_y.$$

Now we list some properties retained by eigenfunctions. First of all as the eigenfunctions are derived from physical flow fields, they too are flow fields. Hence they retain the incompressibility property [Ball et al., 1990], $\nabla \cdot \mathbf{\Psi}^{(\mathbf{k})} = 0$ and satisfy the no-slip boundary conditions, $\mathbf{\Psi}^{(\mathbf{k})} = 0$ at $x_2 = \pm h$. Also if we define the index conjugation as $\overline{\mathbf{k}} = [-k_x, -k_z, q]$ then

$$\mathbf{\Psi}^{(\overline{\mathbf{k}})} = \overline{\mathbf{\Psi}}^{(\mathbf{k})}.$$

As mentioned earlier, the possible uses of the generated empirical eigenfunction-eigenvalue pairs are, storage of the flow field in a compressed manner (only eigenfunction-coefficient pairs should be stored, which is a huge decrement in storage requirements), and the generation of "rather" low dimensional models ([Aubry et al., 1988], [Sirovich and Zhou, 1994]).

We should note that, the tendency to produce truely low dimensional models using a dynamical system of low order ($\mathcal{O}(10)$) have generated controversy. These models may provide insight provided that one views these models as idealizations. It must not

be forgotten that results obtained from such models (and indeed higher dimensional ones) are qualitative. In claiming a low dimensional model tracks NS equations, one asserts that the strange attractor on which the solution field lies (if we assume such an attractor exists for solution fields to NS equations) is in the space spanned by the KL modes used. Current estimates on attractor dimension, however, produced figures like 780 degrees of freedom for $R_\tau = 780$. This number renders all efforts for a low dimensional quantitative description of wall turbulence rather futile. However one does not need to represent all modes to gain insight to the underlying dynamics. So we conclude that "rather" low dimensional models are a valuable tool for qualitative analysis of wall turbulence.

As we mentioned earlier, the KL mode expansion, used in this work, is performed on the full flow field. This is due to the fact that, the mean-fluctuating component seperation, and seperate modelling of the mean flow which appers in (3.2), causes the quadratically nonlinear NS equations be represented by a cubically nonlinear reduced system of ODEs and this causes inconsistencies.

4.3 Symmetries

Channel flow is translationally invariant in longitudinal, x, and lateral, z, directions. Due to the invariance in these directions if, the 4-dimensional velocity field $\mathbf{u}(\mathbf{x}, t)$ solves (3.4), then the field $\mathbf{u}(\, x + L_x \,,\, y \,,\, z + L_z \,,\, t \,)$ is also a solution for any L_x and L_z. It follows from this argument that, the Fourier basis provides the natural represantation of $\mathbf{u}$ in the (x, z) space. Furthermore, the flow field $\mathbf{u}$, reflected in the mean-planes $y = 0$ ($\mathbf{Ref_y}$) or $z = 0$ ($\mathbf{Ref_z}$), or rotated by π about the x-axis ($\mathbf{Rot_x}$), all generate additional solutions to Eqns. (3.4) and make up a symmetry group which

is composed of four elements. To visualize this situation let $\mathbf{v}$ be a vector in a six dimensional space of the from,

$$\mathbf{v} = [x, y, z, u, v, w]^T,$$

then the four elements of the group can be represented in matrix form by,

$$\begin{aligned}
\mathbf{Ref_y} &= diag[1, 1, -1, 1, 1, -1] \quad &\Longrightarrow \quad \mathbf{Ref_y}\,\mathbf{v} &= [x, y, -z, u, v, -w], \\
\mathbf{Ref_z} &= diag[1, -1, 1, 1, -1, 1] \quad &\Longrightarrow \quad \mathbf{Ref_z}\,\mathbf{v} &= [x, -y, z, u, -v, w], \\
\mathbf{Rot_x} &= diag[1, -1, -1, 1, -1, -1] \quad &\Longrightarrow \quad \mathbf{Ref_z}\,\mathbf{v} &= [x, -y, -z, u, -v, -w],
\end{aligned}$$

resulting in the symmetry group

$$\mathcal{G} = \{\mathbf{I}, \mathbf{Ref_y}, \mathbf{Ref_z}, \mathbf{Rot_x}\}$$

Where $\mathbf{I}$ is the identity transformation, and note that $\mathbf{Rot_x} = \mathbf{Ref_y}\mathbf{Ref_z}$. The symmetries have been introduced into the computation of the KL eigenfunctions through the extension of the ensemble size by 4 fold via group actions [Sirovich et al., 1991, Sirovich et al., 1990a]. Since KL decomposition is a statictical procedure, the size and representation quality of the underlying ensemble plays a crucial role on the sharpness of the resulting KL modes. The extensions of the ensemble via symmetries contributes to this objective. Thus the KL eigenfunctions come with a degeneracy of maximum 4, i.e

$$\lambda^q(m, n) \;=\; \lambda^q(m, -n) \;=\; \lambda^q(-m, n) \;=\; \lambda^q(-m, -n).$$

This suggests that eigenfunction calculations are only necessary for positive values of (m, n). Others belonging to the same family of $\{m, n\}$,

$$\{m,n\} = \{\underbrace{(m,n),(-m,-n)}_{\text{conjugate pairs}};\ \underbrace{(m,-n),(-m.n)}_{\text{conjugate pairs}},\}$$

can be generated by group actions

$$\mathbf{Ref_y}[m,q,n,\Phi_1,\Phi_2,\Phi_3]^T = [m,q,-n,\Phi_1,\Phi_2,-\Phi_3]^T,$$
$$\mathbf{Ref_z}[m,q,n,\Phi_1,\Phi_2,\Phi_3]^T = [-m,q,n,-\Phi_1,\Phi_2,-\Phi_3]^T,$$
$$\mathbf{Rot_z}[m,q,n,\Phi_1,\Phi_2,\Phi_3]^T = [-m,q,-n,-\Phi_1,\Phi_2,-\Phi_3]^T.$$

In the light of these symmetry considerations, the KL decomposition of the flow can be written as in terms of the *flowlets*, $\mathbf{u_m}$

$$\mathbf{u_m}(\mathbf{x},t) = \underbrace{a_{mqn}(t)\mathbf{\Psi}^{(\mathbf{m,q,n})}(x) + a_{-mq-n}(t)\mathbf{\Psi}^{(\mathbf{-m,q,-n})}(x)}_{\text{conjugate pairs}} +$$
$$\underbrace{a_{-mqn}(t)\mathbf{\Psi}^{(\mathbf{-m,q,n})}(x) + a_{mq-n}(t)\mathbf{\Psi}^{(\mathbf{m,q,-n})}(x)}_{\text{conjugate pairs}}$$

having physical attributes.

4.4 Mode Families

The KL modes are classified into three groups [Ball et al., 1990]. The *roll* modes, which have $m = 0$, are independent of the longitudinal coordinate, and represent streamwise rolls (hence the name). These modes are directly linked to streaks and

mainly confined to the wall region. The *propagating* modes, have streamwise dependence ($m \neq 0$), and have their main support in the core region, we further classify these modes as *core-modes*, $(m, 0, q)$, and *(oblique) waves*, (m, n, q). The last class of modes is the so called *net-flux* mode familiy, which receive the forcing, and mimic the mean flow. Wavenumbers in homogenous coordinates (m, n) range , $0 \leq |m|, |n| \leq 5$, the quantum number (q) belongs to the interval $1 \leq q \leq 25$. In total there are $6 \times 6 \times 25 = 900$ stored modes, the total number of modes created via group actions is 3025. The cutt-off index has been determined by searching the index for which the reconstructed flow field retains more than %90 of the original energy. A short list of energy fractions for a number of modes is given in Table 4.1. It is obvious that most of the energy resides in the net-flux modes as the KL modes are extracted from the full flow field.

The modes except the net-flux family exhibit, quantum number parity,for example $k(m, n, 1)$ is even, and $k(k_x, k_z, 2)$ is the corresponding odd function. Due to this parity the mode selection always involves an even number of quantum layers.

It is also worthwhile to note that the for roll mode $(0, 1, 1)$, the center of the roll closest to the wall is approximately at the maximum turbulence production location $(y^+ \approx 12)$, while the propagating mode $(1, 0, 1)$ has the main activity in the core.

Table 4.1: Energy fractions of KL modes.

Mode (m,n,q)	$\sqrt{\frac{\lambda_m^2}{E}}$	Mode (m,n,q)	$\sqrt{\frac{\lambda_m^2}{E}}$
0 0 1	0.99997759	1 0 5	0.000212495752
0 1 1	0.00475737681	2 1 2	0.00019530793
0 1 2	0.0037529525	2 0 2	0.000192116994
0 1 3	0.00105245305	0 1 5	0.000189426314
0 0 2	0.000959730622	0 1 6	0.000187764969
0 0 3	0.000958763048	2 0 3	0.000182640943
1 1 1	0.000871290228	1 0 6	0.000178927105
1 1 2	0.000861367446	0 0 8	0.000158498939
0 1 4	0.000777764922	0 0 9	0.000156747012
0 0 4	0.000739000196	1 1 5	0.000147032156
0 0 5	0.000531445248	2 0 4	0.000138155178
0 2 1	0.000493009909	0 1 7	0.000138046068
1 0 1	0.000483169474	1 1 6	0.000134863367
1 0 2	0.000367204683	2 1 3	0.000121747591
1 1 3	0.000340297887	1 0 7	0.00011491487
1 0 3	0.000330045718	0 0 10	0.000112477407
1 1 4	0.000308265006	0 0 11	9.80482E-05
1 0 4	0.000303530069	1 0 8	9.62098091E-05
2 1 1	0.000295810063	0 2 3	9.5254587E-05
0 0 6	0.000282963972	0 2 4	9.4906672E-05
0 0 7	0.000273782311	3 1 1	9.38855725E-05
0 2 2	0.000271785402	3 0 1	9.35664789E-05
1 2 1	0.000238002654	3 0 2	8.95911902E-05
1 2 2	0.000230982595	2 1 4	8.89756483E-05
2 0 1	0.000217642423	1 0 9	8.88191895E-05

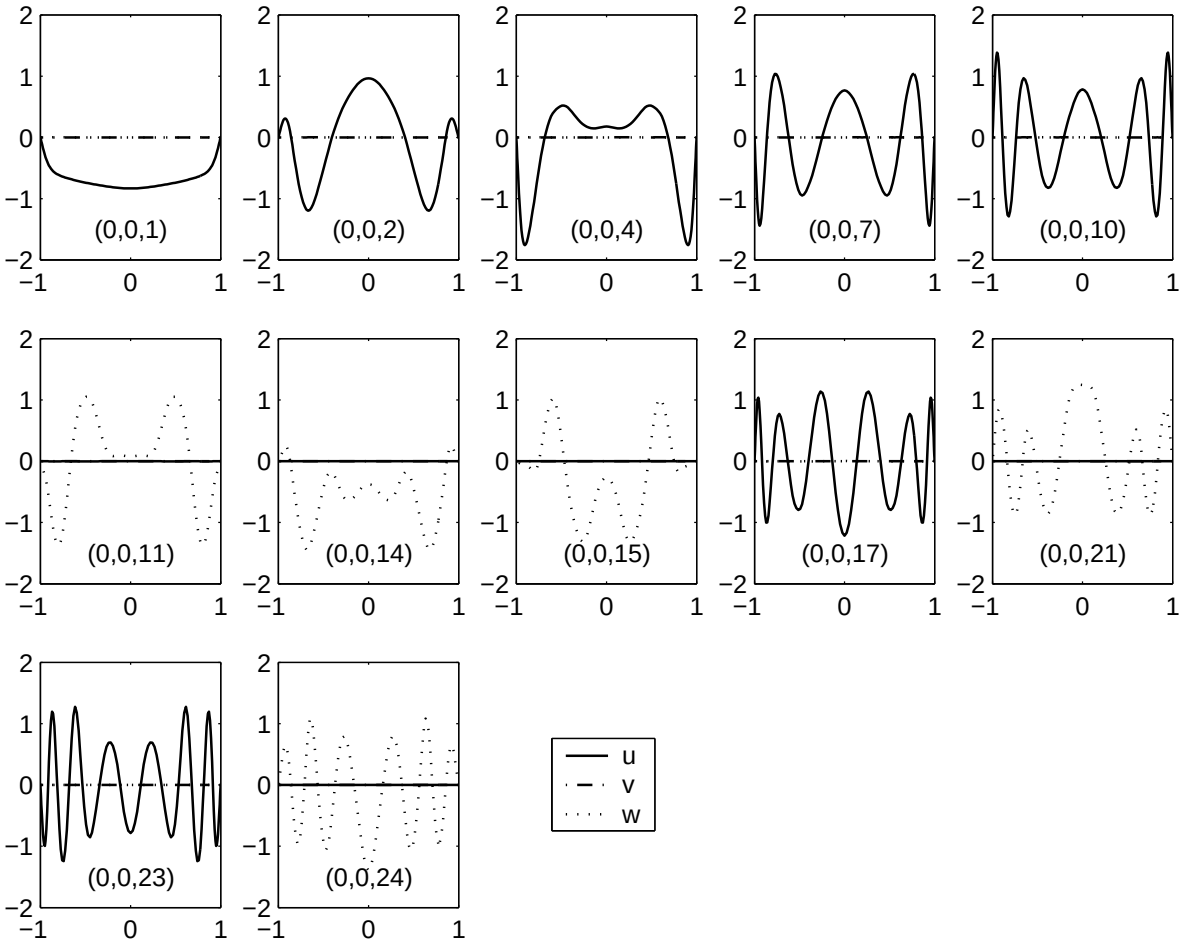

Figure 4.1: Net-flux (mean flow) KL modes.

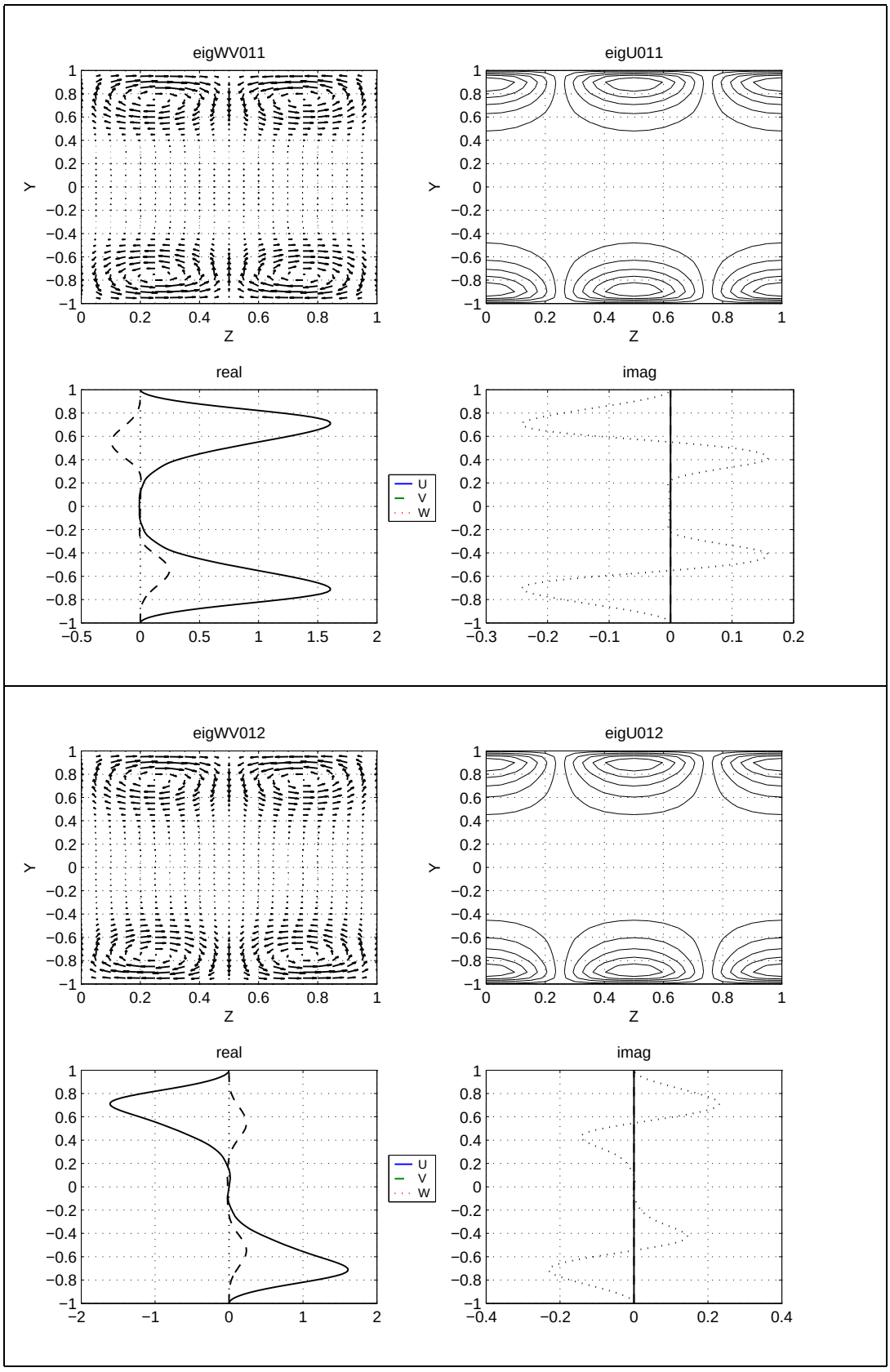

Figure 4.2: Roll (KL) modes $\mathbf{\Phi}^{(0,1,1)}$ and $\mathbf{\Phi}^{(0,1,2)}$.

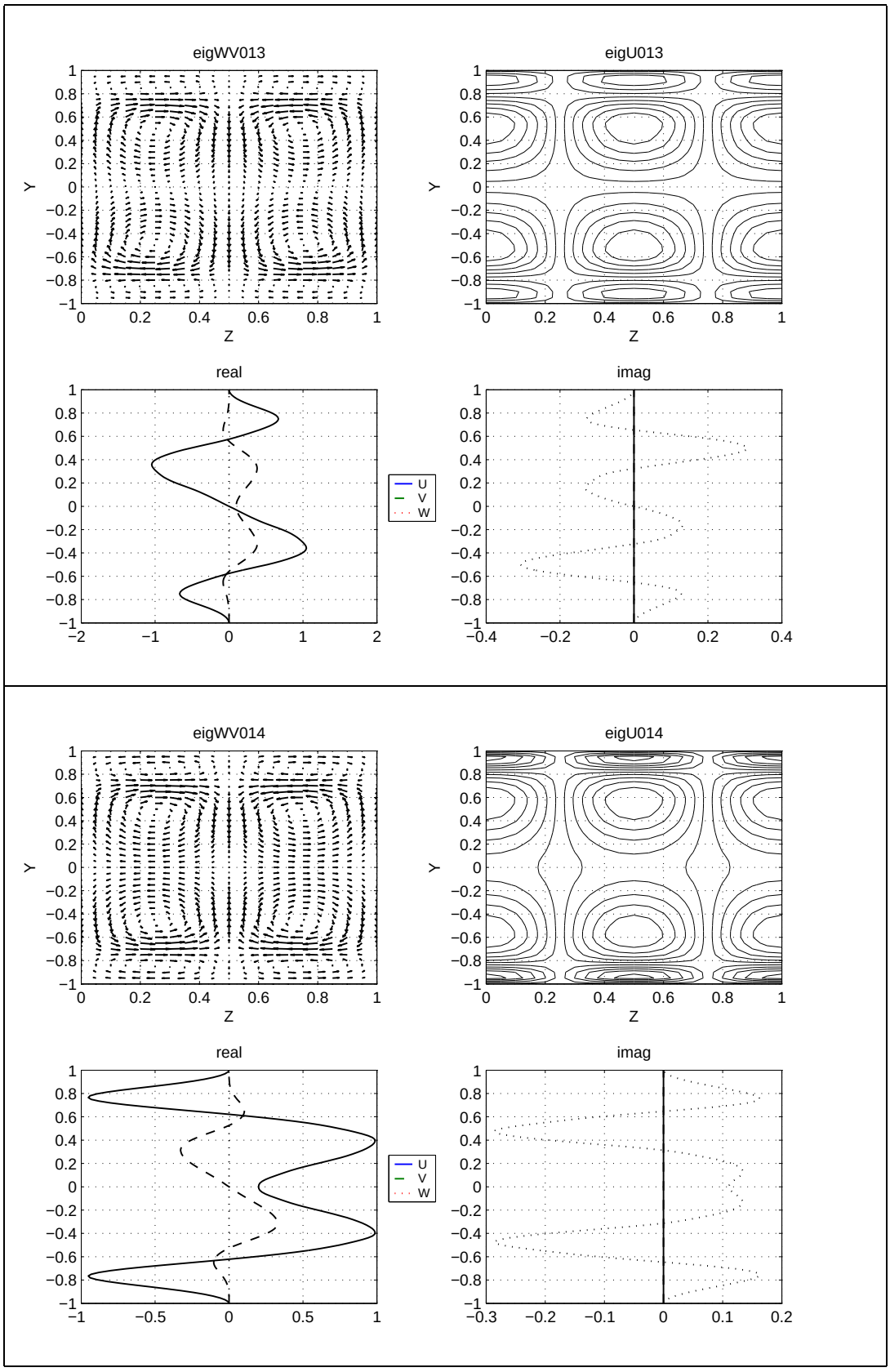

Figure 4.3: Roll (KL) modes $\mathbf{\Phi}^{(0,1,3)}$ and $\mathbf{\Phi}^{(0,1,4)}$.

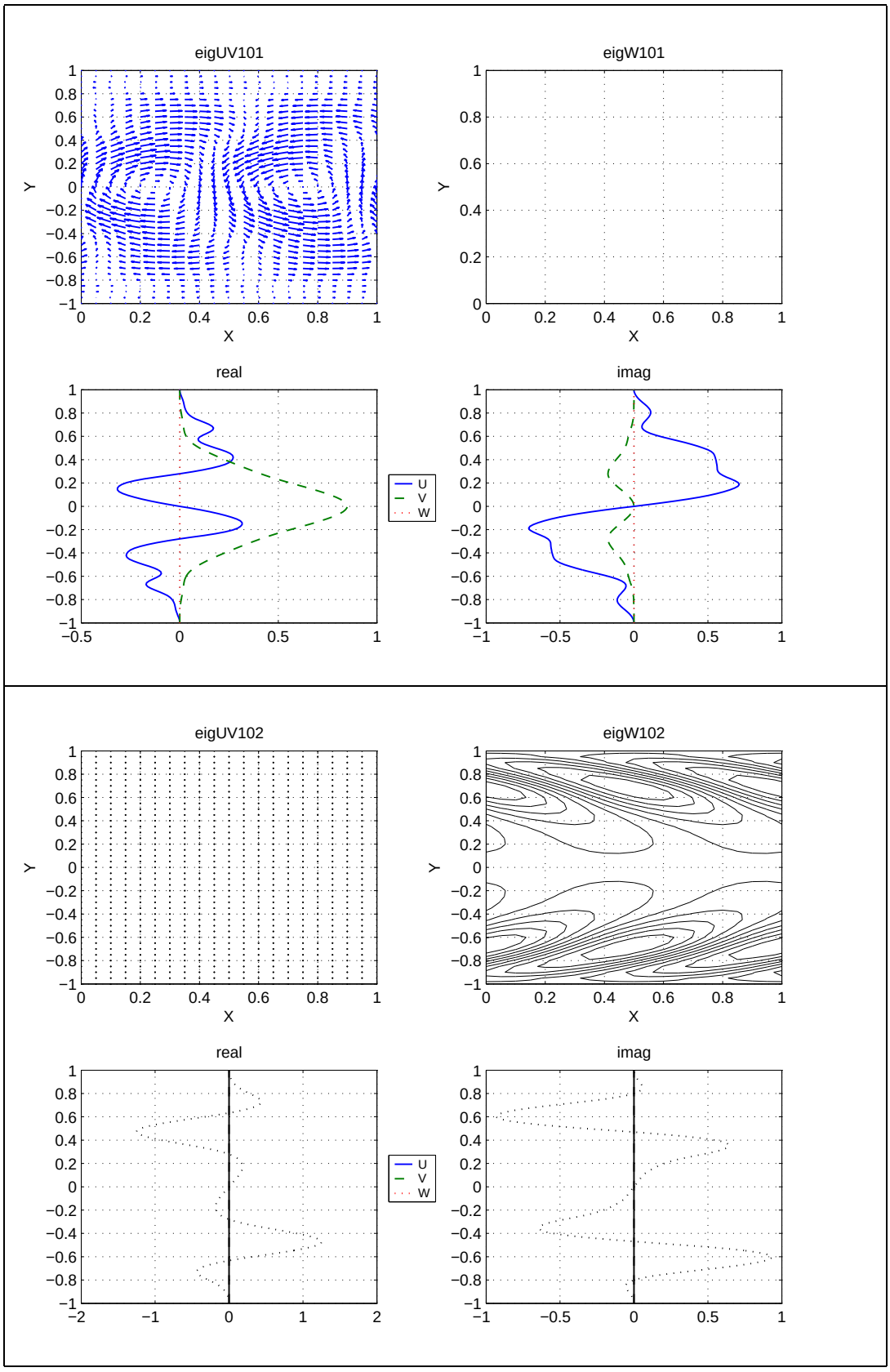

Figure 4.4: Propagating (KL) modes $\mathbf{\Phi}^{(1,0,1)}$ and $\mathbf{\Phi}^{(1,0,2)}$ a.k.a. cores modes.

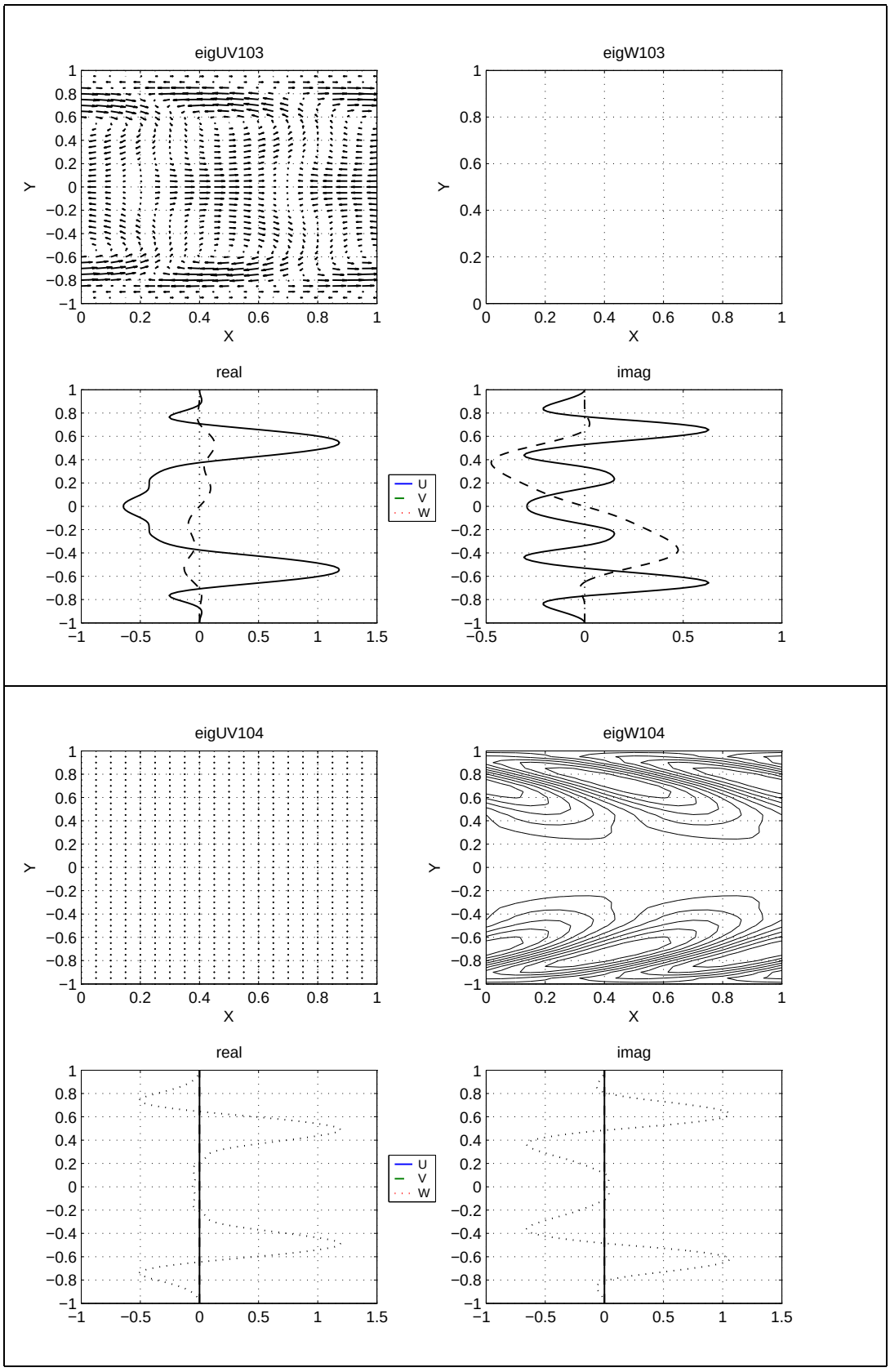

Figure 4.5: Propagating (KL) modes $\mathbf{\Phi}^{(1,0,3)}$ and $\mathbf{\Phi}^{(1,0,4)}$ a.k.a. core modes.

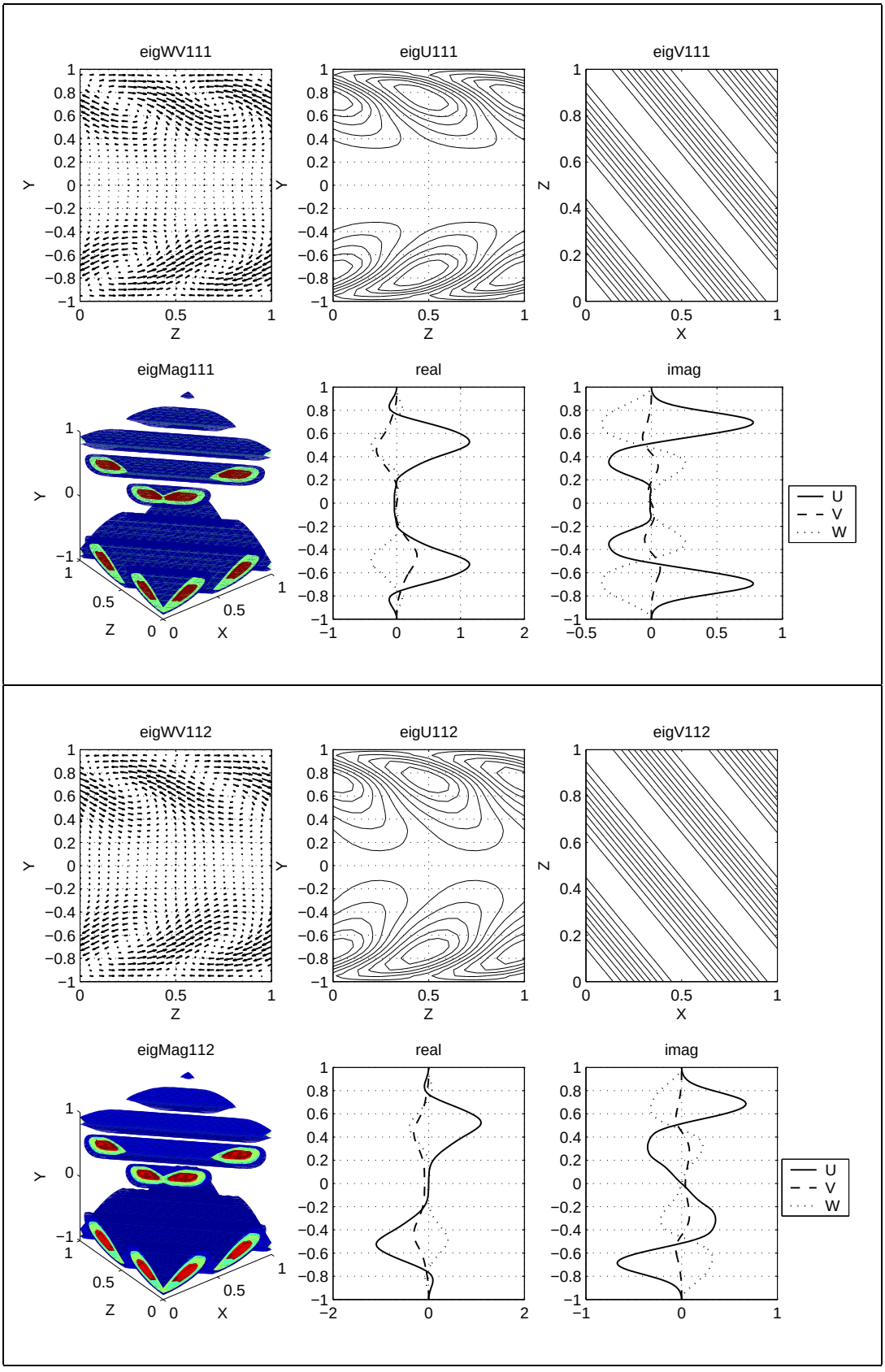

Figure 4.6: Propagating (KL) modes $\mathbf{\Phi}^{(1,1,1)}$ and $\mathbf{\Phi}^{(1,1,2)}$.

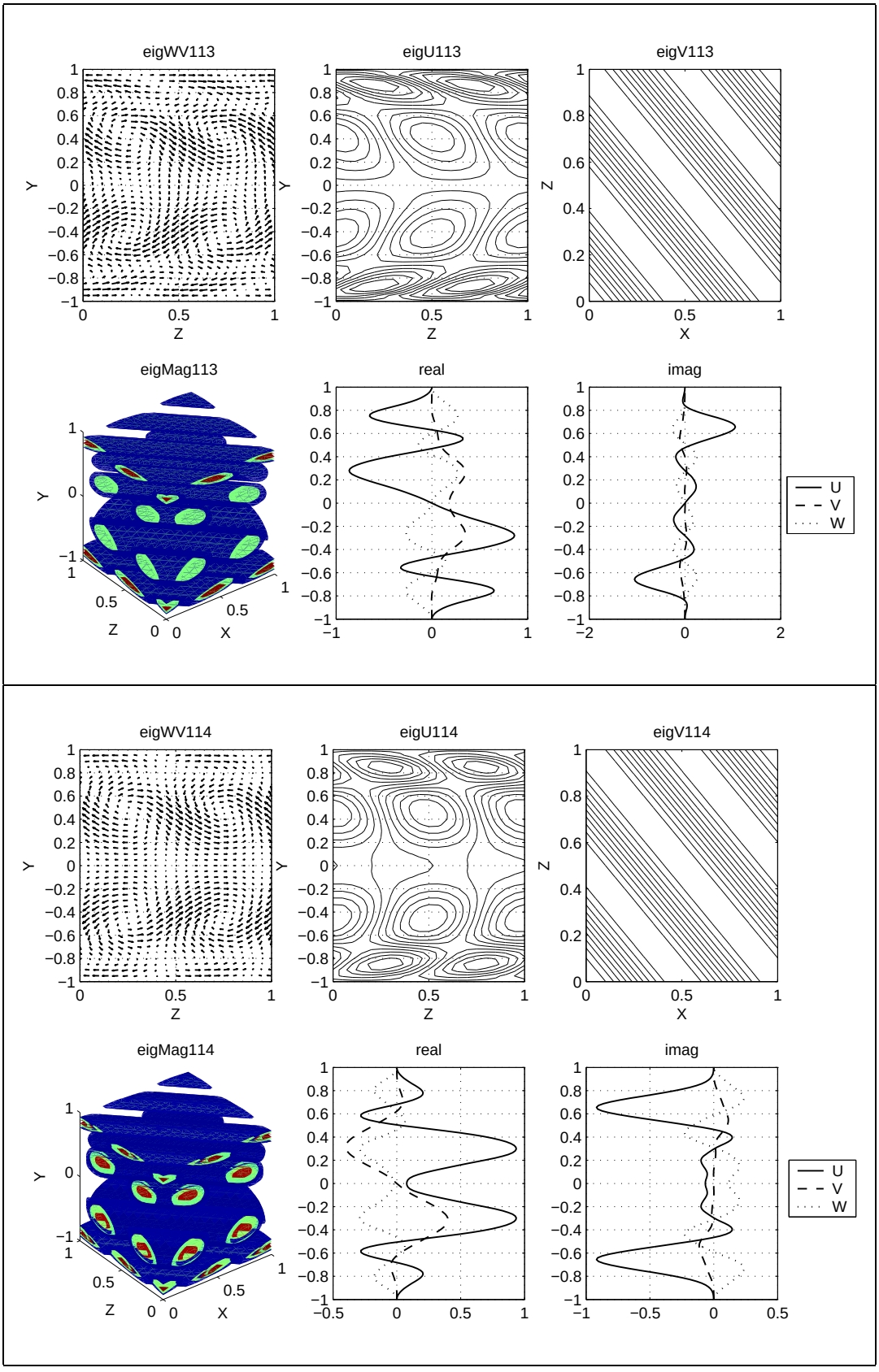

Figure 4.7: Propagating (KL) modes $\mathbf{\Phi}^{(1,1,3)}$ and $\mathbf{\Phi}^{(1,1,4)}$.

CHAPTER 5

THE NUMERICAL MODEL

5.1 Preliminaries

The computer code employed was written in FORTRAN 77 with FORTRAN 90 like extensions available through GNU's g77 compiler. A number of libraries are also used (namely *blas* and *rksuite* [Brankin et al., 1993]; which are obtainable through `http://www.netlib.org`). The code was written for GNU/Linux systems, and is not portable without modification of the output routine (which uses `time()` system call to create output directories).

Briefly, the code first calculates the coefficients of the coupled ODE resulting from the projection of NS equations onto the subspace spanned by the selected KL modes. This is followed by a time integration of the resulting set of ODEs.

In chapter 4,we have presented the KL expansion applied to channel flow. The development involved the seperation of the flow field into *mean* and *fluctuating* components. The KL-modes then, were obtained from the fluctuating portion of the flow. In this approach, one needs seperate integraton of mean and fluctuating components.

As mentioned earlier, this in turn results in an inconsistent time dependence for the mean flow and cubic-direction-field (in KL coefficients a_k).

So it is convenient to construct the KL-basis using the total flow field. The procedure to obtain the emprical eigenfunctions corresponding to the full flow field, from the eigenfunctions constructed form the fluctuating velocity field, is relatively simple. First observe that mean flow is only dependant on the wall normal coordinate (recall that $U(y)\delta_{i1}$). Thus it is void of dependence on x and z coordinates. If we consider the structure of the KL-modes, as given by (4.5) in page 31, we can easily conclude that only those modes with both $k_x = 0$ and $k_z = 0$ will be different than the modes for the fluctuating portion.

5.2 Galerkin Projection

Galerkin projection is a common method in computational science and engineering, so only problem specific information is presented here. We first start subtituting the KL represantation of the velocity field (given by 4.6) into the normalized NS equations (eqn. 3.4) [Webber et al., 2002] resulting in

$$\sum_{\mathbf{r}} \frac{d}{dt} a_{\mathbf{r}} \, \mathbf{\Psi^{(r)}} = -\left(\sum_{\mathbf{p}} a_{\mathbf{p}} \, \mathbf{\Psi^{(p)}} \right) \cdot \nabla \left(\sum_{\mathbf{q}} a_{\mathbf{q}} \, \mathbf{\Psi^{(q)}} \right) - \nabla p + \frac{1}{R_\tau} \nabla^2 \left(\sum_{\mathbf{p}} a_{\mathbf{p}} \, \mathbf{\Psi^{(p)}} \right) + \mathbf{e_1}$$

To obtain a set of coupled differential equations for the coefficients for $a_{\mathbf{k}}(t)$, the Galerkin projection is used. This is nothing but the projection of the above expression onto the subspace spanned by the KL eigenfunctions (which can be written as $span\{\mathbf{\Psi^{(k)}}\}$). The projection is done via the weighted discrete inner product defined

earlier (see eqn. 4.7, page 32). Performing the projection and rearranging one gets,

$$\frac{d}{dt}a_{\mathbf{k}} = -\sum_{\mathbf{p}}\sum_{\mathbf{q}} a_{\mathbf{p}}a_{\mathbf{q}}\left(\mathbf{\Psi^{(p)}}\cdot\nabla\mathbf{\Psi^{(q)}},\mathbf{\Psi^{(k)}}\right)_{\omega}+\frac{1}{R_\tau}\sum_{\mathbf{p}} a_{\mathbf{p}}(\Delta\mathbf{\Psi^{(p)}},\mathbf{\Psi^{(k)}})_{\omega}+(\delta_{i1},\mathbf{\Psi^{(k)}})_{\omega},$$

Note that in the above equation the term involving the pressure term drops due to the periodicity of the pressure field and the eigenfunctions together with the fact that the eigenfunctions are incompressible and zero along surfaces $y = \pm 1$.

If we define the coefficients $prod, diss, nlin$ as:

$$prod_{(\mathbf{k})} = (\delta_{i1},\mathbf{\Psi^{(k)}})_{\omega}$$
$$\text{if} \quad k_x = 0 \quad \text{and} \quad k_z = 0$$

$$diss_{(\mathbf{k};\,\mathbf{p})} = \frac{1}{R_\tau}(\Delta\mathbf{\Psi^{(p)}},\mathbf{\Psi^{(k)}})_{\omega}$$
$$\text{if} \quad k_x = p_x \quad \text{and} \quad k_z = p_z$$

$$nlin_{(\mathbf{k};\,\mathbf{p},\mathbf{q})} = -\left(\mathbf{\Psi^{(p)}}\cdot\nabla\mathbf{\Psi^{(q)}},\mathbf{\Psi^{(k)}}\right)_{\omega}$$
$$\text{if} \quad k_x = p_x + q_x \quad \text{and} \quad k_z = p_z + q_z$$

The resulting equations become:

$$\frac{d}{dt}a_{\mathbf{k}} = prod_{(\mathbf{k})} + \frac{1}{R_\tau}diss_{(\mathbf{k};\,\mathbf{p})}a_{\mathbf{p}} + nlin_{(\mathbf{k};\,\mathbf{p},\mathbf{q})}a_{\mathbf{p}}a_{\mathbf{q}},$$

(summation convention on repeated indices). In the above quations k ranges over the selected index set of conjugate pairs **indxv**(the full set has 3025 modes with 1525 conjugate-pairs) whereas p and q range over the full selected set **cindexv**. Note that

k, p, q are actually vectors corresponding to (kxs(k),kzs(k),mds(k)).

5.3 Program details

Prior to the execution of the program, a list of selected KL modes is stored in a file, this file is then fed to the main program. After the selected mode list is read, the program creates the coefficients $nlin, diss, prod$, sets up the coupled system of nonlinear differential equations and calls the integrating routine. The mode list presented to the program does not involve those modes which are complex conjugates of each other, these modes are formed by a subroutine called ***dynsys_cindex()***.

The integration is handled by a subroutine called ***ut*** belonging to ***rksuite***, which is an adaptive step size Runge-Kutta integrator, and can also handle mildly stiff differential equations. The integration is carried on about 10^5 time steps after the initial transients are discarded (on a simple Reynold number based criteria). The step size used is 10^{-3}, halving the step size does not yield any significant change in the results. More information about the integrator can be found at the *netlib repository* (`http://www.netlib.org`). The data is sampled every 50 timesteps. Over %95 of total CPU time is consumed by the integrating routine.

The KL-representation of a parabolic velocity profile is taken to be the initial condition. If the integration is to be performed over a Reynolds number range, the initial condition corresponding to the first Reynolds number is taken to be the corresponding parabolic profile, in the following Reynolds numbers, the time average velocity profile for the previous Reynolds number is perturbed and used as an initial condition. Use of random initial conditions results in no perceptible change in qualitative behaviour.

As mentioned earlier the equations for $a_{\mathbf{k}}(t)$ are only solved for a single member

of a conjugate family $(a_{\mathbf{k}}, a_{\overline{\mathbf{k}}})$ (consult page 32, for index conjugation). This can geometrically be viewed as the integration being carried out only for quadrants I and IV, or quadrants II and III in the wave number space (m, n). In our program quadrants I and IV are chosen (purely for cosmetic reasons, the outcome of the integration would be identical independent of the quadrants considered). The other member in the conjugate family is equal to the complex conjugate of the calculated member. This conjugate property roughly halves the calculation costs .

The code runs as follows:

- Read the index vector containing the quadrants I and IV, in wave number space (m, n).
- Generate the full index vector, containing the indexes read and their conjugate indexes
- Read input files, read *prod* coefficient-index matrix
- Calculate and store *diss* and *nlin* coefficient-index matrices
- Enter Reynolds number loop (if exists)
- Initialize the solution by projection of a parabolic profile initially, afterwards disturb the previous solution
- Enter solution loop

In pseudo-code:

```
  PROGRAM dynsys_main
  read indxv            !read in the selected modes
  call dynsys_cindex    !create full index set
  call dynsys_init      !read in Diff. matrices,eigenfunctions etc.
  call dynsys_coeff     !create dissipation and nonlinear coefficients
  call dynsys_init_mode !assign initial values to a_k
  call setup            !initialize the integration routine

  for the Reynolds number range:
  do i=1,nstep
     call ut              !integrate the equations
     call dynsys_entropy    !calculate entropy,
     call dynsys_energy_prop !energies in mode families
     if steady-state then
       conduct average in time
     endif
  enddo

  call dynsys_vel_ave     !reconstruct flow field
  call dynsys_slope_check  !check slope at y={1,-1}
  call out_put              !output the solution etc.
  END PROGRAM dynsys_main

  subroutine dynsys_init()
  read Dy,D2y            !read in Chebyshev diff matrices order 1&2
  read fa{x,z},fac{x,z}  !read in wave number arrays
  read e{u,v,w}{r,i}     !read in K-L eigenfunctions
  read k{x,z}{s,p}       !read in index-vector values (kx,kz,mds)
  read mds,mndex
  read cprod(indxv)      !read in the production coefficients
                         !corresponding to the selected set.
 end subroutine dynsys_init

 subroutine dynsys_coeff()
 do ik=1,nmod         !loop over the selected modes,number=nmod
    do ip=1,len_cin   !loop over full selected set,number=len_cin
       call dyndiss   !calculate the dissipation coeff. (ik;ip)
    end do
 end do

do ik=1,nmod          !loop over the selected modes,number=nmod
   do ip=1,len_cin
      do iq=1,len_cin
         call dynnlin    !calculate nlin coeff .(ik;ip;iq)
      enddo
   enddo
enddo
end subroutine dynsys_coeff
```

5.4 Validation

We run our model as a test, in a laminar setting. By laminar setting, it is understood all the modes included in the selection are initialized as zero. As the forcing is only on the so-called net-flux modes, we expect only the net-flux modes evolve and then evolve to result in the parabolic profile. This setting can be thought as an idealized channel flow, where there exist no perturbations of any kind.

In table 5.1, we present the slope of the velocity profile, at an xy-crosssection with $z = 0$, at the walls. The exact value of these slopes is known to be $\pm R_\tau$. Table 5.2 gives the comparison of the calculates centerline velocity with the theoretical value of $R_\tau/2$, and a comparison of the calculated and the exact results.

Table 5.1: Slope of velocity profile at the walls, laminar setting

Exact,R_τ	upper wall	lower wall	% error
20	-19.7730631	19.7730632	1.1347
40	-39.5474857	39.5474858	1.1313
60	-59.3212291	59.3212293	1.1313
80	-79.0949778	79.094978	1.1313
100	-98.8687412	98.8687414	1.1313

Table 5.2: Velocity profile, laminar setting

R_τ	exact	DS	% error U_{CL}	$\frac{\|u_{\text{exact}}-u\|_\infty}{U_{CL}}$
20	10	9.9294	0.71	0.0083134
40	20	19.860	0.70	0.0082703
60	30	29.789	0.70	0.0082703
80	40	39.719	0.70	0.0082702
100	50	49.649	0.70	0.0082699

Clearly our model produces the well known parabolic profile for an ideal setting. This gives us the initial confidence necessary for further utilization the model.

CHAPTER 6

RESULTS and CONCLUSIONS

The computer code simulating the model was run for different paramaters, such as Reynolds number, the truncation cut-off. Obviously the most important parameter of the problem is the number and nature of the retained KL modes. The model is used to predict the qualitative behaviour in the region where transition to turbulence occurs. Each selected mode subset (each different model ODE system for turbulence), was run on a Reynolds number range. While selecting the modes, the odd-even parity was taken into account so that number of quantum layers (the y component in index space) is always even.

For benchmarking purposes we compare the ratio of maximum velocity to mean velocity,$(u^*_{centerline}/u^*_{average})$, and velocity defect ratio $(u^*_{centerline} - u^*_{average})$, with those graphed in [Dean, 1978]. The effect of mode selection on velocity defect ratio is given in figure 6.2

Clearly the model captures the qualitative aspects of the transition but lacks the accuracy in predicting the region of transition. However the selection of modes only weakly affects the drop of velocity defect ratio as long as the mode parity is taken into account (by using an even number of quantum numbers).

Also, qualitatively speaking, independent of the mode selection a periodic region followed by a quasiperiodic region is observed before the chaotic regime. Tests are performed both using random and parabolic initial (i.e. corresponding laminar velocity profile) conditions. The initial conditions corresponding to presented results is parabolic profile for the first Reynolds number, perturbation of the previous result for

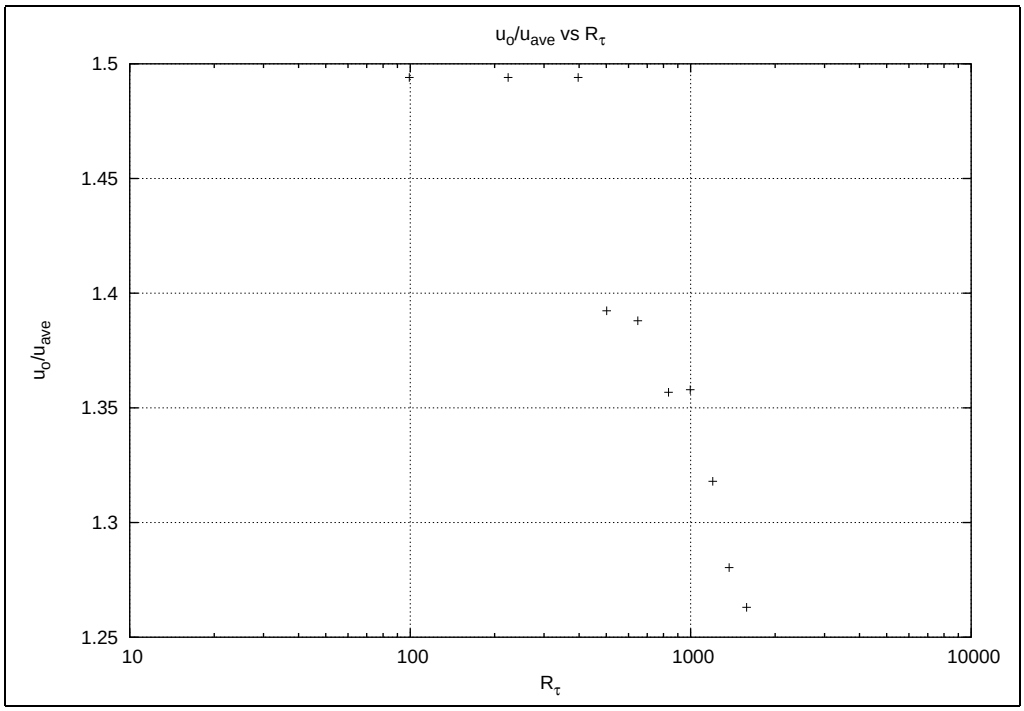

Figure 6.1: Velocity ratio, rectangular mode selection=2x2, 10 quantum layers.

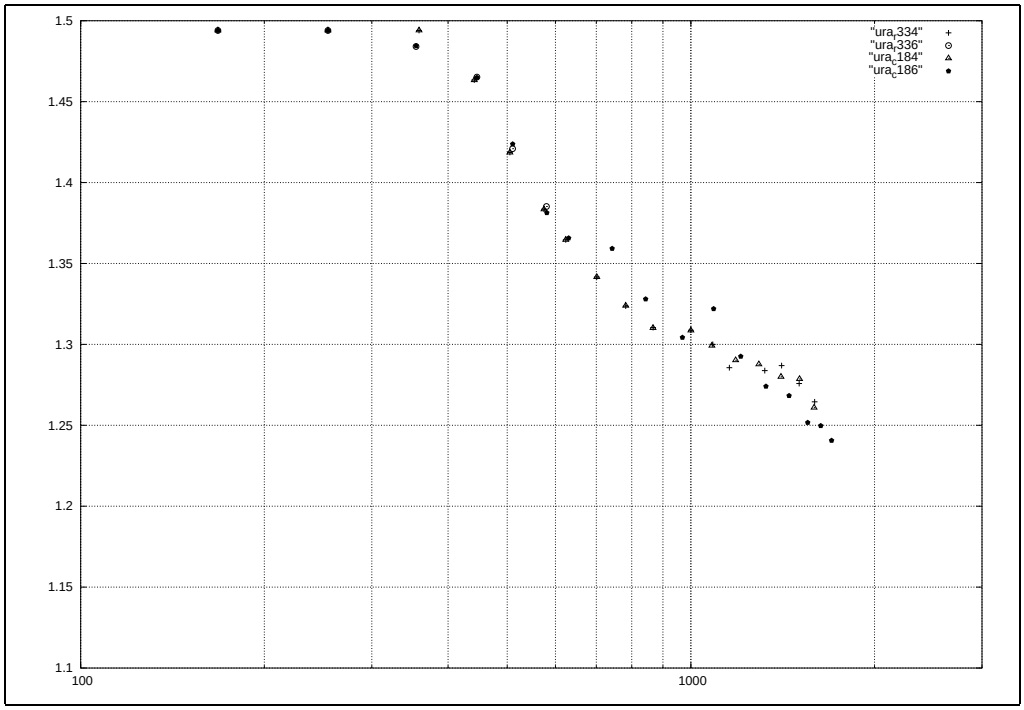

Figure 6.2: Velocity ratio, various mode selections.

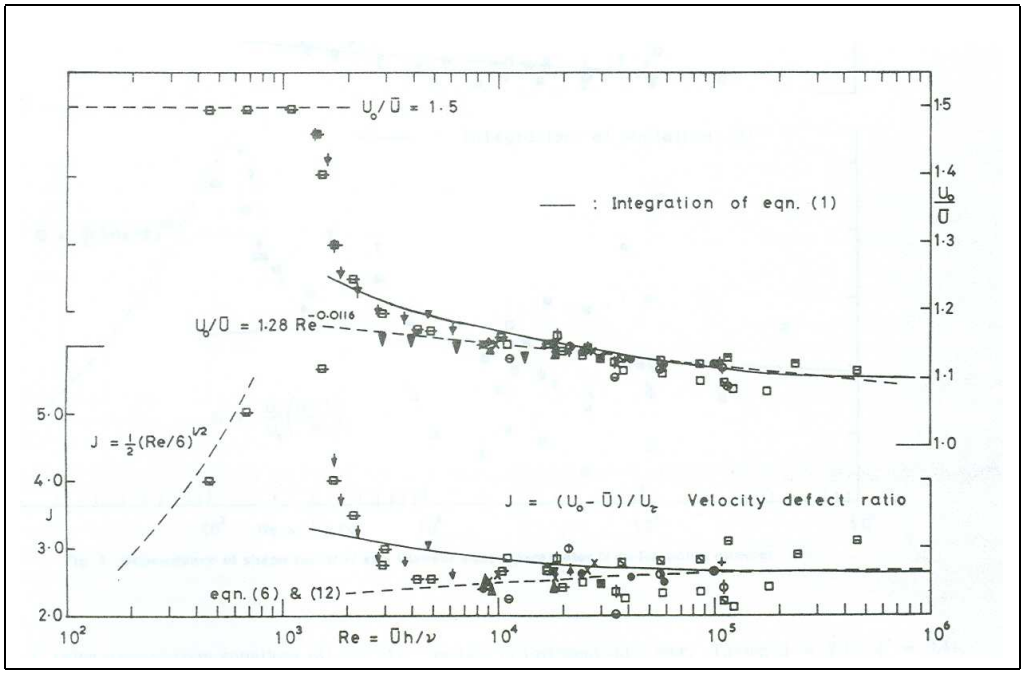

Figure 6.3: Original plot of the experimental data complied by Dean [Dean, 1978].

the other Reynolds numbers.

The representational (or Shannon) entropy, plotted in figure 6.9, is a measure of lack of information about the flow. The entropy increases as the energy is distributed among modes. For a totally stochastic system one would observe the energy fraction of the modes be almost equal (white noise). The Shannon entropy is defined as:

$$S(p) = -\sum_{i=1}^{N} p_i \ln p_i \tag{6.1}$$

Where p_i is the realtive frequency of event i, in our case the relative energy of the mode i $(a_i a_i^c / \sum a_i a_i^c)$. Note that $S(p)$ is always positive and has a maximum at $\ln N$. For an excellent account on thermodynamics approach to complex system, see [Beck and Schlögl, 1995]

The above graphs, illustrate transition from laminar flow to turbulence, it is clear as R_τ is increased the signals (time histories of velocity components) approach white noise. But as observed from figure 6.9 the magnitude of the Shannon entropy is less than that for a fully stochastic [1].

[1] Had the system been stochastic the Shannon entropy would have been around 3.9

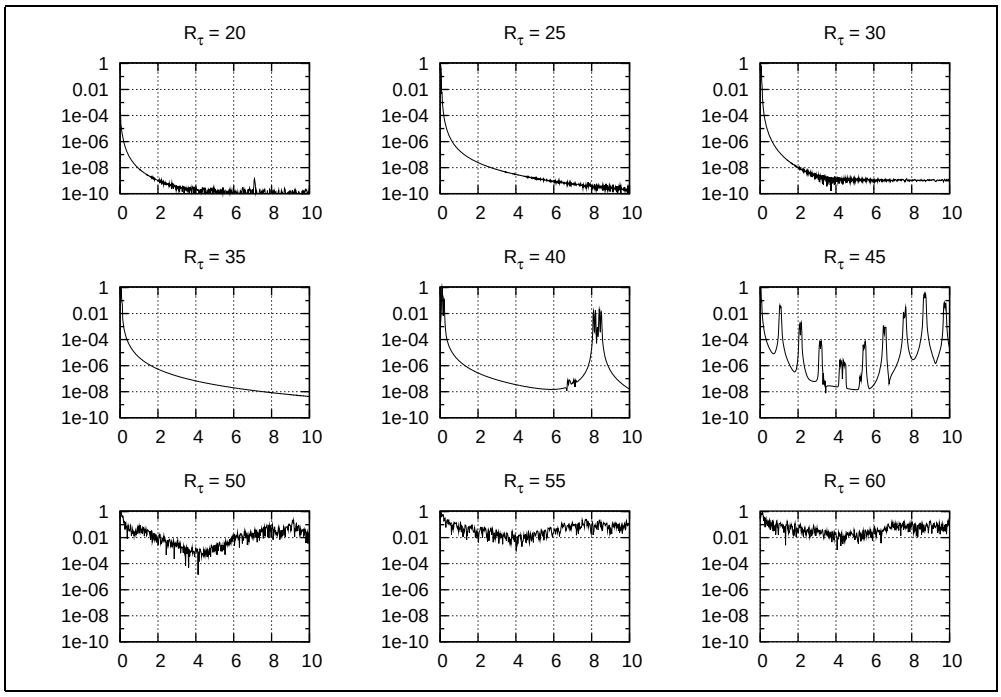

Figure 6.4: FFT of u-velocity signal, rectangular mode selection 2x2, quantum layers=4. At $(0, -0.9, 0)$.

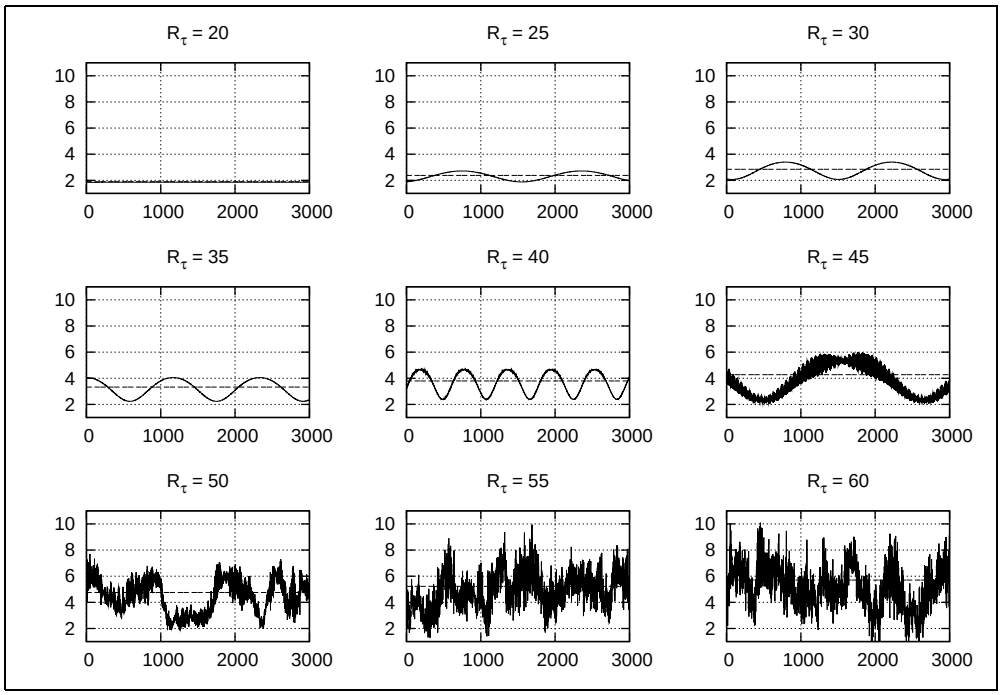

Figure 6.5: u-velocity time signal, rectangular mode selection 2x2, quantum layers=4, corresponds to figure 6.4. Dashed lines: u-velocity for the laminar case.

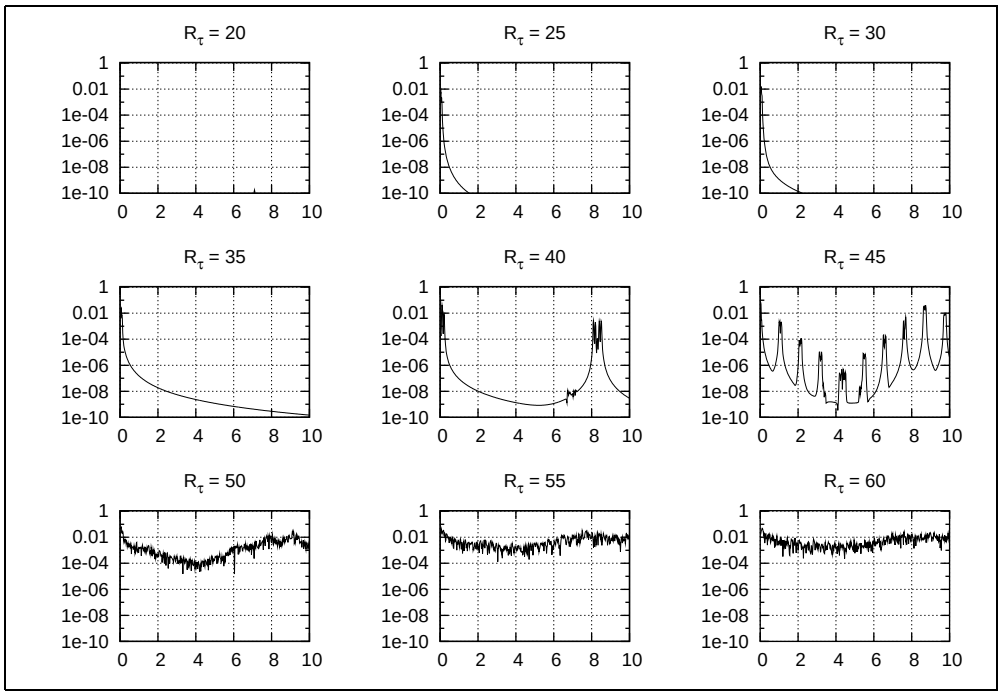

Figure 6.6: FFT of v-velocity signal, rectangular mode selection 2x2, quantum layers=4. At $(0, -0.9, 0)$.

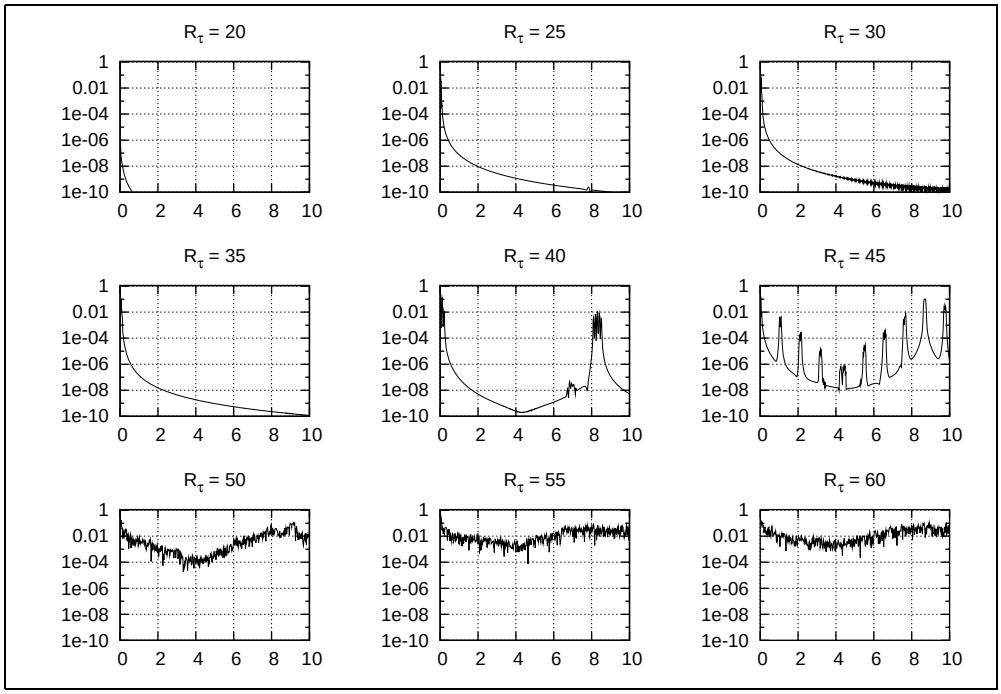

Figure 6.7: FFT of w-velocity signal, rectangular mode selection 2x2, quantum layers=4. At $(0, -0.9, 0)$.

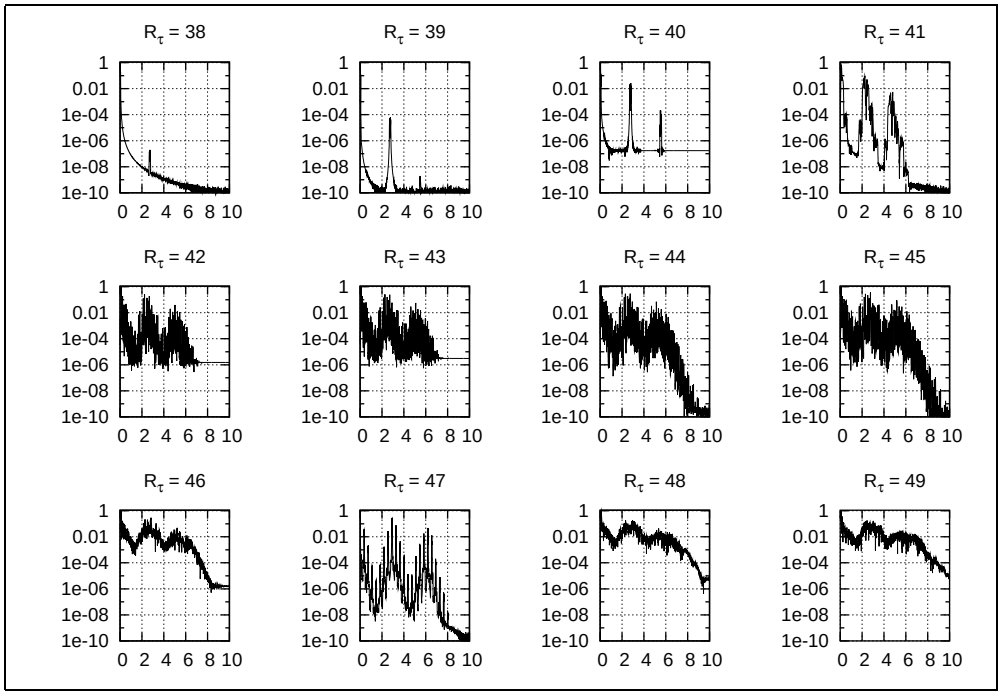

Figure 6.8: FFT of w-velocity signal, rectangular mode selection 2x2, quantum layers=4. Close-up on the transition region. At $(0, -0.9, 0)$.

As the number of quantum layers is increased the transition region is pushed to lower Reynolds numbers. In the experiments, it is observed the transition region lays in the range $R_\tau^{cr} \in (35, 55)$, an interval which is not far away from the experimental value of $R_\tau^{cr} \simeq 62$. The transition is reached following a periodic and a quasiperiodic region. After the transition, the turbulent activity switches from wall to wall, which is in accordance with other numerical experiments [Webber et al., 1997, Jiménez and Moin, 1990].

The onset of turbulent activity can also be observed from the Reynolds stress, as presented in figure 6.10

In line with the Squire's theorem, two-dimensional modes are more sensitive to perturbations, perturbations on roll and core $(m, 0, q)$ modes are amplified at lower Reynolds number. Also the amplification factors for 2D disturbances are higher. In a simulation where no selective disturbances are given, first the roll-modes gain energy from the mean flow. The roll-modes are followed by core modes and oblique-waves. At roughly the point where the wave modes experience a relatively large energy increase, the flow becomes turbulent. Figure 6.11 shows the periodic and quasiperiodic regions.

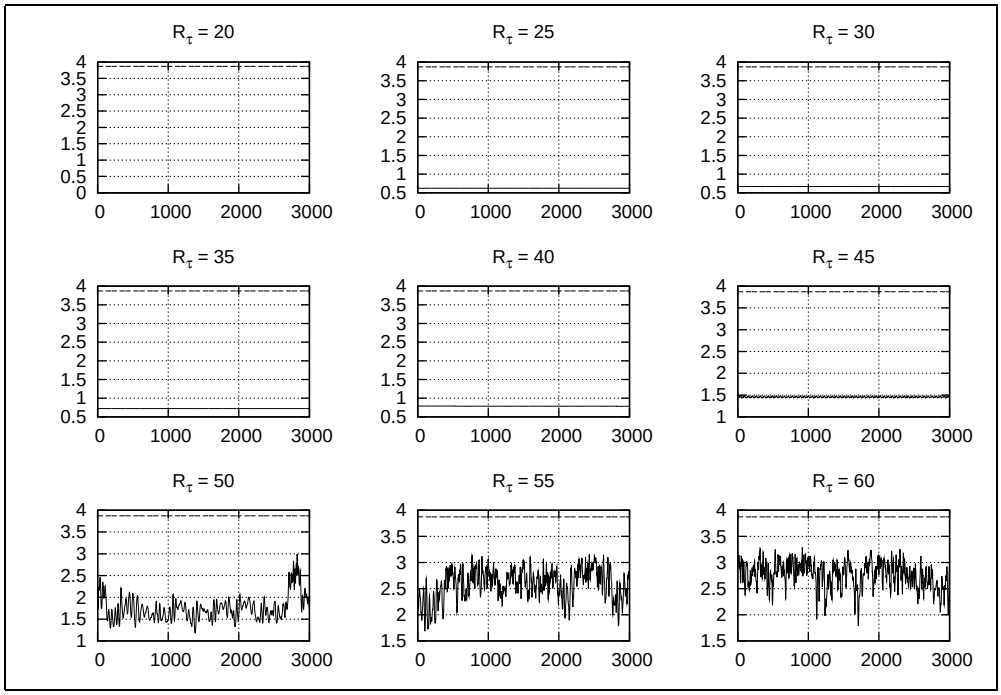

Figure 6.9: Representational entropy time signal, rectangular mode selection 2x2, quantum layers=4, corresponds to figure 6.4. Dashed lines: maximum possible Shannon-entropy for the mode selection.

We can clearly observe the transition in figure 6.14, where as R_τ is increased from 39 to 40, the roll modes experience an amplification of $\mathcal{O}(100)$.

The energy exchange between roll and propagating families is evident from figures 6.15 and 6.16

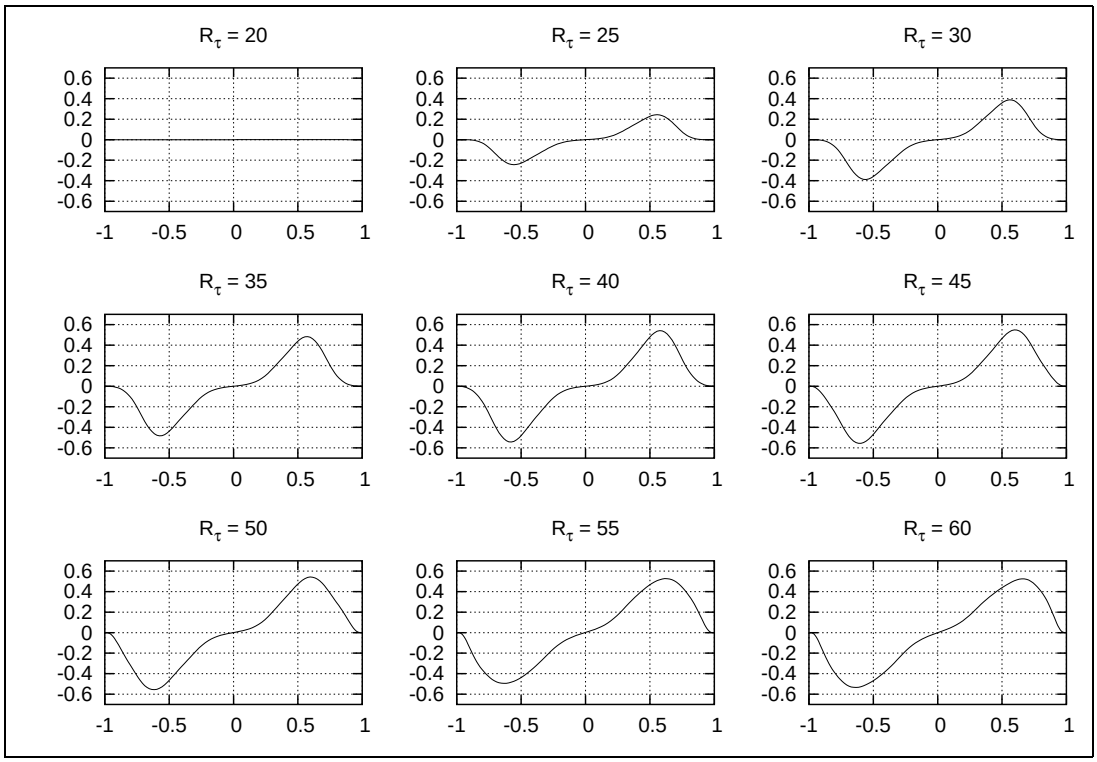

Figure 6.10: Reynolds stress rectangular mode selection 2x2, quantum layers=4.

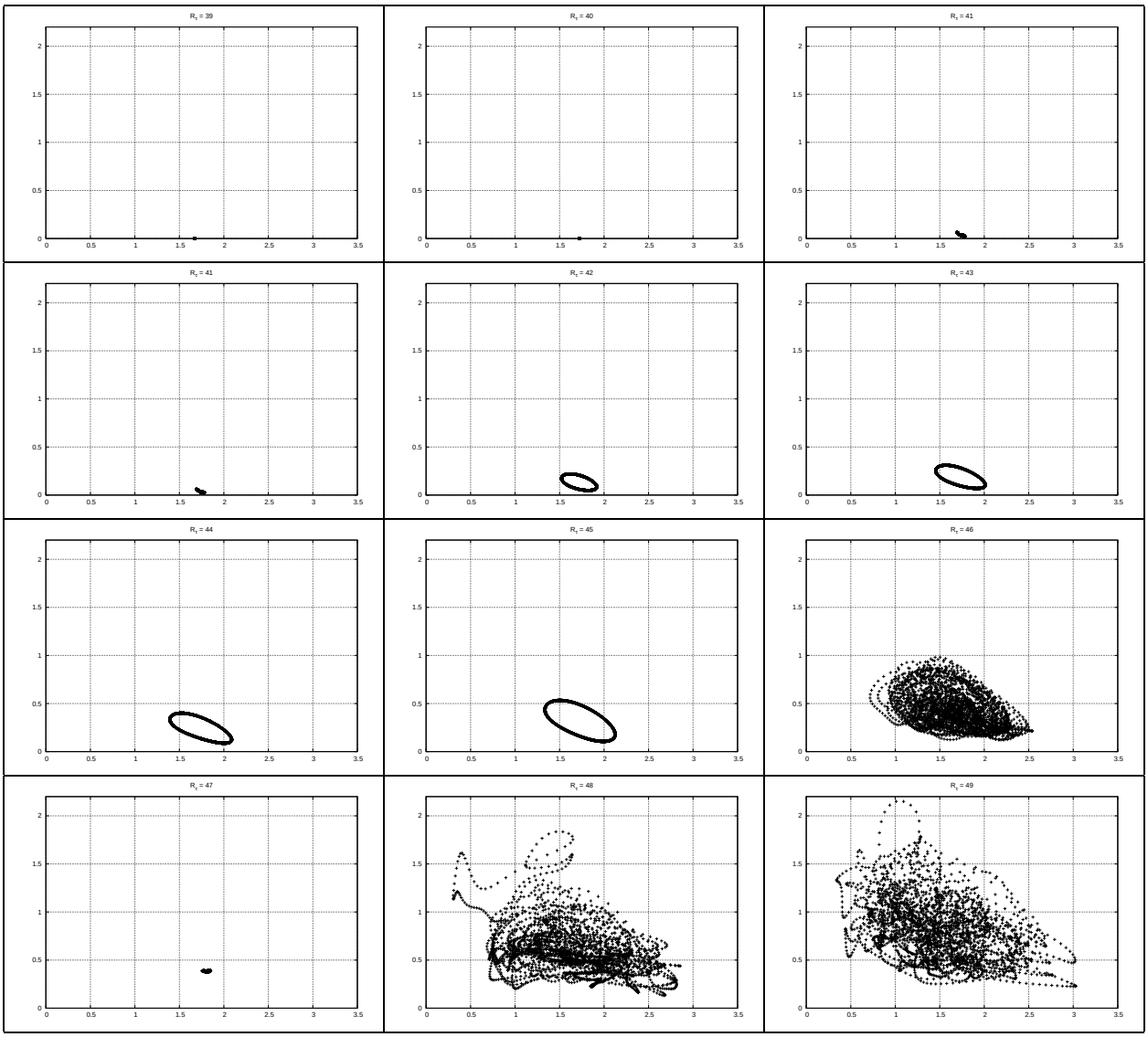

Figure 6.11: Propagating mode energy versus roll energy, mode selection 2x2, quantum layers=4, top left $R_\tau = 39$ increments of $R_\tau = 1$, right-bottom.

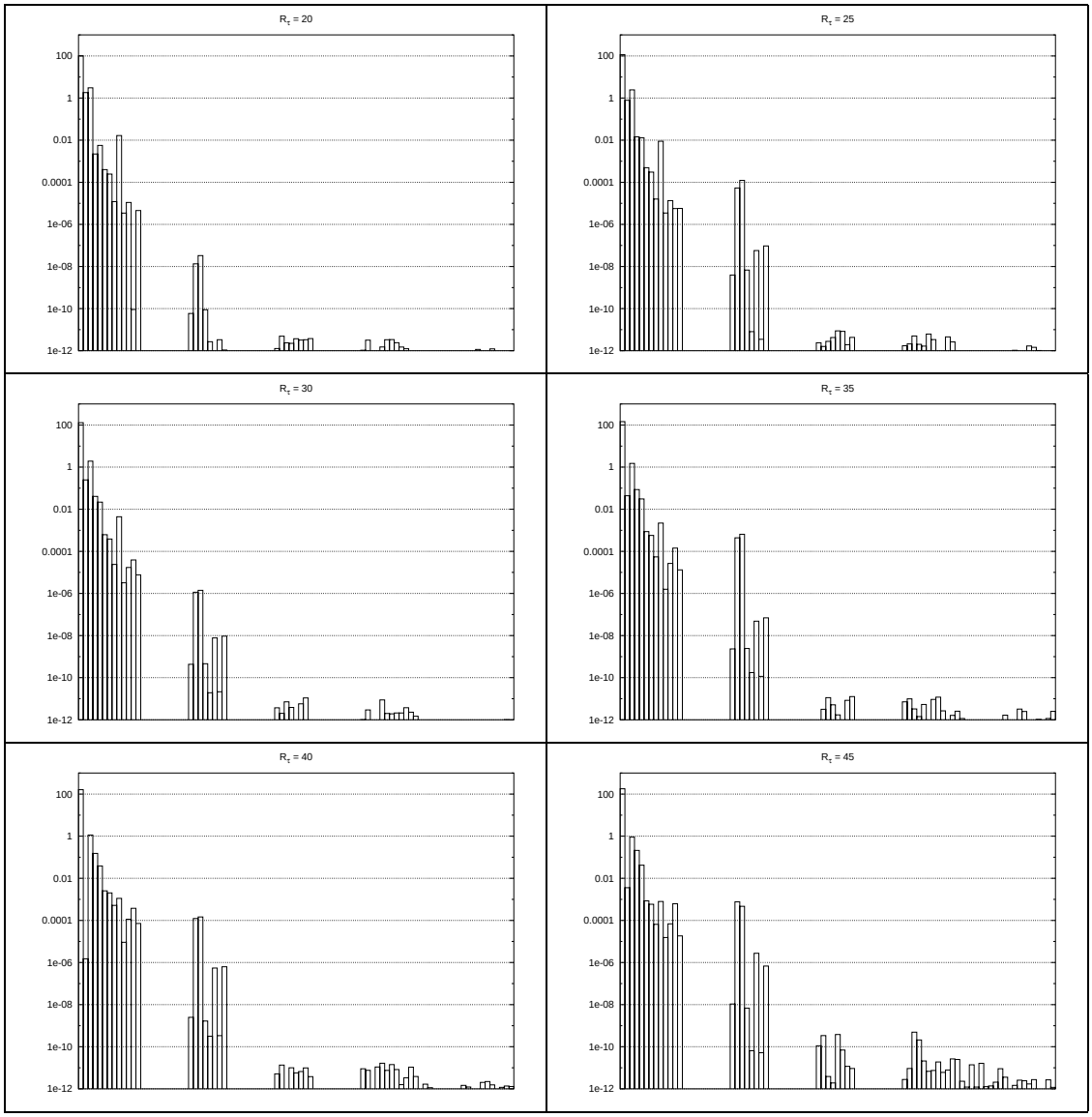

Figure 6.12: Production, roll, core, wave mode energies. The groups correspond to production, roll, core, wave modes respectively from left to right.

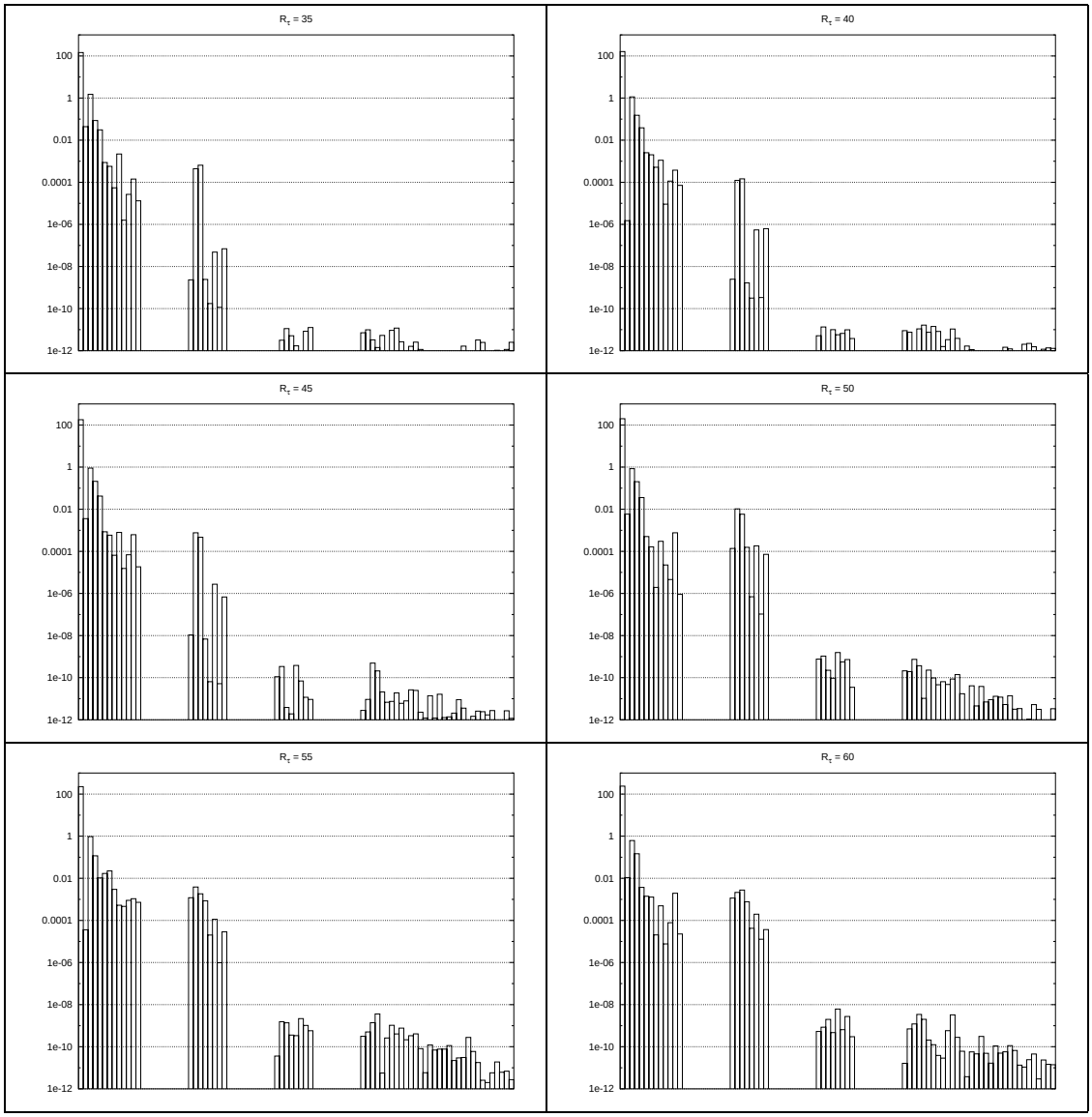

Figure 6.13: Production, roll, core, wave mode energies. The groups correspond to production, roll, core, wave modes respectively from left to right.

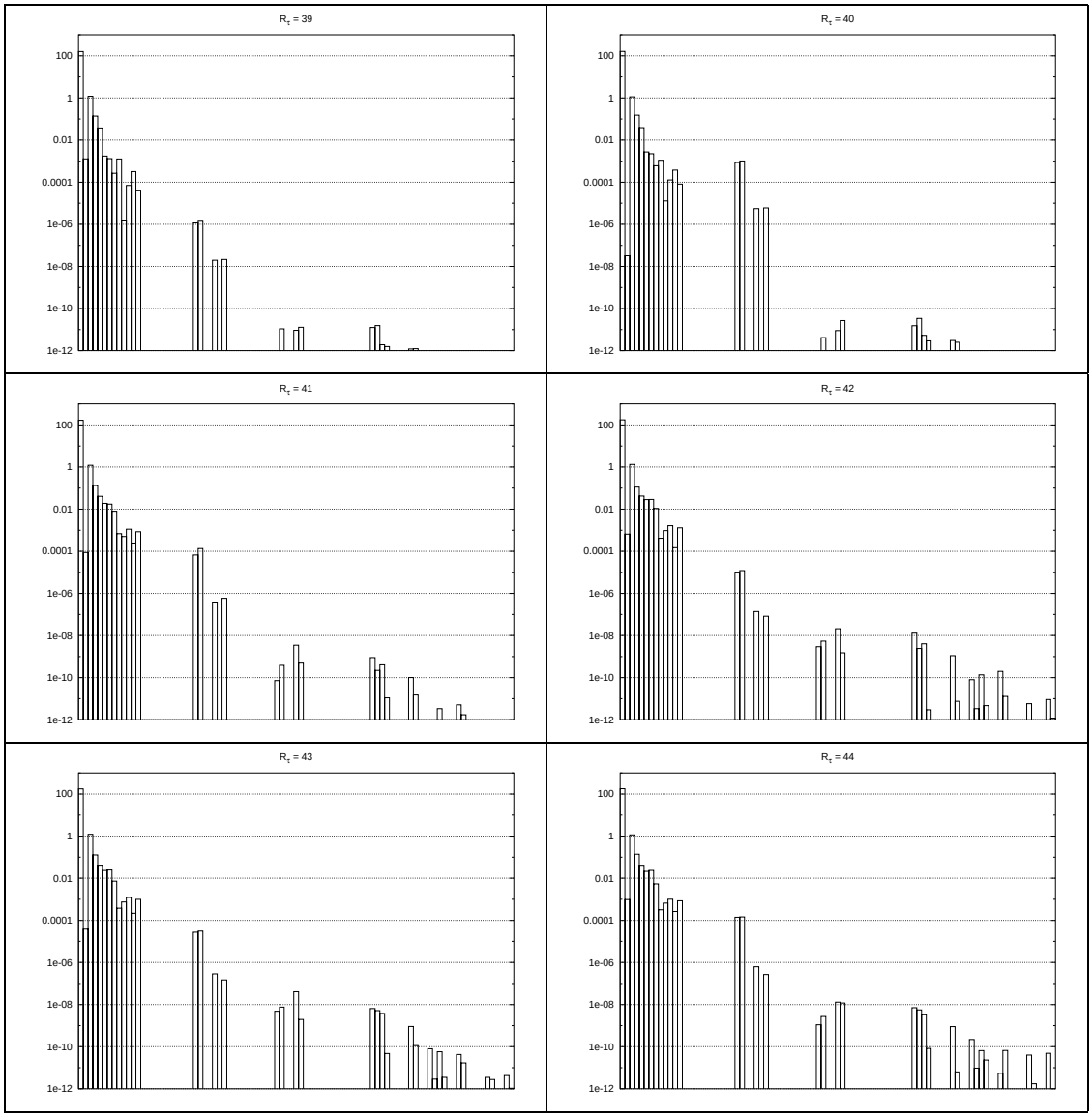

Figure 6.14: Production, roll, core, wave mode energies. The groups correspond to production, roll, core, wave modes respectively from left to right. Close up on transition region.

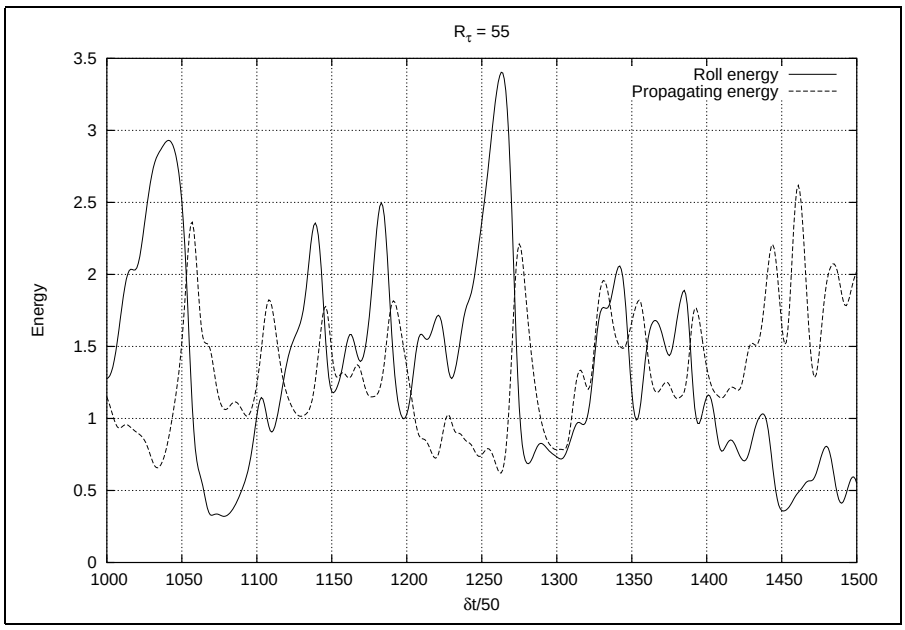

Figure 6.15: Energy exchange between mode families, rectangular mode selection 2x2, quantum layers=4, $R_\tau = 55$.

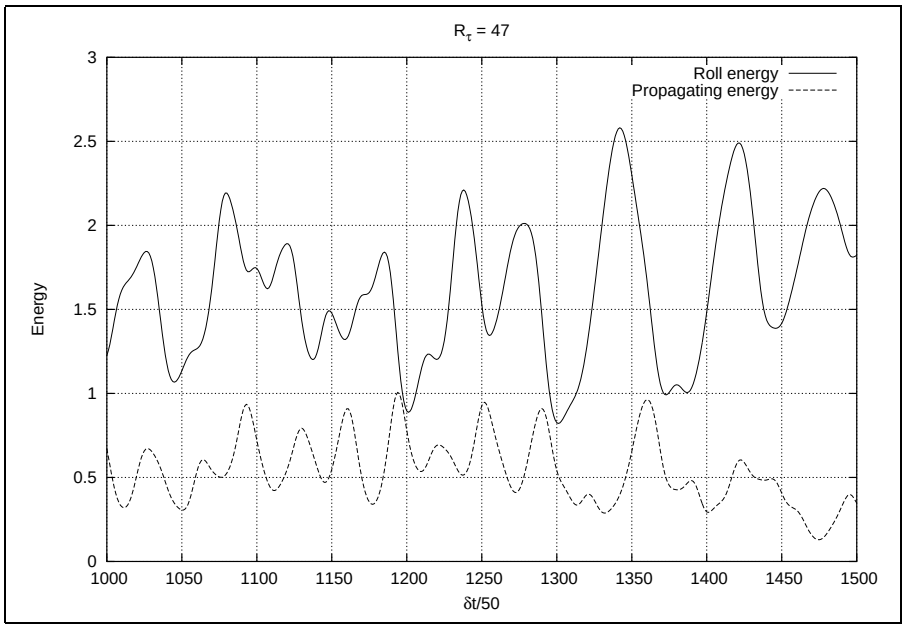

Figure 6.16: Energy exchange between mode families, rectangular mode selection 2x2, quantum layers=4, $R_\tau = 47$.

6.1 Future Work

The work presented here can be extended/enhanced in a number of ways. We list these possible extensions/enhancements in order of relative simplicity.

- Pseudospectra analysis can be performed and the results can be compared to Orr-Sommerfeld equations. Further the spectrum can be used to verify/identify mode sets which represent better models for the NS equations in the given domain.

- Turbulence control can be attempted by selectively exciting/repressing certain modes, probably with the help of machine learning algorithms (i.e. artifical neural networks, evolution strategies.)

- DNS if turbulence on a finer grid can be performed (possibly at a Reynolds number closer to transition). From the data obtained, a new KL-basis can be computed. The presented study, then, can be repeated with the new set of KL eigenfunctions and the results can be compared.

REFERENCES

[Aubry et al., 1988] Aubry, N., Holmes, P., Lumley, J. L., and Stone, E. (1988). The dynamics of coherent structures in the wall region of turbulent boundary layer. *Journal of Fluid Mechanics*, 192:115.

[Ball et al., 1990] Ball, K. S., Sirovich, L., and Keefe, L. R. (1990). Dynamical eigenfunction decomposition of turbulent channel flow. *International Journal for Numerical Methods in Fluids*, 12:585–604.

[Beck and Schlögl, 1995] Beck, C. and Schlögl, F. (1995). *Thermodynamics of chaotic systems, an introduction*. Cambridge University Press.

[Brankin et al., 1993] Brankin, R., Gladwell, I., and Shampine, L. (1993). RKSUITE: A Suite of Explicit Runge-Kutta Codes. In Agarwal R. P., editor, *Contributions to Numerical Mathematics*. World Scientific.

[Cantwell, 1981] Cantwell, B. J. (1981). Organized motion in turbulent flows. *Ann. Rev. Fluid Mech.*, 13:457–515.

[Dean, 1978] Dean, R. B. (1978). Reynolds number dependence of skin friction and other bulk flow variables in two-dimensional rectangular duct flow. *Journal of Fluids Engineering*, 100:215–221.

[Drazin and Reid, 1981] Drazin, P. G. and Reid, W. H. (1981). *Hydrodynamic stability*. Cambridge University Press.

[Fukanaga, 1972] Fukanaga, K. (1972). *Introduction to Statistical Pattern Recognition*. Academic Press.

[Guckenheimer, 1986] Guckenheimer, J. (1986). Strange attractors in fluids: Another view. *Ann. Rev. Fluid Mech.*, 18:15–32.

[Holmes et al., 1998] Holmes, P., Lumley, J. L., and Berkooz, G. (1998). *Turbulence, coherent structures, dynamical systems, and symmetry*. Cambridge University Press.

[Jiménez, 2003] Jiménez (2003). Computing high-Reynolds-number turbulence: will simulations ever replace experiments. *Journal of Turbulence*, 4:1–3.

[Jiménez and Moin, 1990] Jiménez, J. and Moin, P. (1990). The minimal flow unit in near-wall turbulence. *Journal of Fluid Mechanics*, 225:213–240.

[Jiménez and Simens, 2000] Jiménez, J. and Simens, M. (2000). Low dimensional dynamics of wall bounded turbulence. *Center for Turbulence Research, Annual Research Briefs.*, pages 67–77.

[Kim et al., 1987] Kim, J., Moin, P., and Moser, R. (1987). Turbulence statistics in fully developed channel flow at low Reynolds number. *Journal of Fluid Mechanics*, 177:133.

[Lumley, 1967] Lumley, J. C. (1967). The structure of inhomogeneous turbulent flows. In Yaglom, A. M. and Tatarski, L., editors, *Atmospheric Turbulence and Radio Wave Propagation*, pages 166–178. Nauka.

[Lumley, 1970] Lumley, J. C. (1970). *Stochastic Tools in Turbulence*. Academic Press.

[Orszag, 1971] Orszag, S. A. (1971). Accurate solution of the Orr-Sommerfeld stability equation. *Journal of Fluid Mechanics*, 50:869.

[Orszag and Kells, 1980] Orszag, S. A. and Kells, L. C. (1980). Transition to turbulence in plane poiseuille and plane couette flow. *Journal of Fluid Mechanics*, 96:159.

[Orszag and Patera, 1983] Orszag, S. A. and Patera, A. T. (1983). Secondary instability of wall-bounded shear flows. *Journal of Fluid Mechanics*, 128:347.

[Preisendorfer, 1988] Preisendorfer, R. W. (1988). *Principal Component Analysis in Meteorology and Oceanography*. Elsevier.

[Reddy et al., 1998] Reddy, S. C., Schmid, P. J., Bagget, J. S., and Henningson, D. S. (1998). On stability of streamwise streaks and transition tresholds in plane channel flows. *Journal of Fluid Mechanics*, 365:269.

[Reddy and Trefethen, 1994] Reddy, S. C. and Trefethen, L. N. (1994). Pseudospectra of the convection-diffusion operator. *SIAM Journal of Applied Mathematics*, 54:1634.

[Riesz and Nagy, 1955] Riesz, F. and Nagy, B. S. (1955). *Functional Analysis*. Ungar.

[Schmid and Henningson, 2001] Schmid, P. J. and Henningson, D. S. (2001). *Stability and transition in shear flows, Applied Mathematical Sciences*, volume 142. Springer Verlag.

[Sirovich, 1986] Sirovich, L. (1986). Turbulence and the dynamics of coherent structures part {I,II,III}: Coherent structures. *Quarterly of Applied Mathematics*, XLV:561–571.

[Sirovich et al., 1991] Sirovich, L., Ball, K. S., and Handler, R. A. (1991). Propagating structures in wall-bounded turbulent flows. *Theor. Comput. Fluid Dyn.*, 2:307.

[Sirovich et al., 1990a] Sirovich, L., Ball, K. S., and Keefe, L. R. (1990a). Plane waves and structures in turbulent channel flow. *Physics of Fluids*, 2:2217.

[Sirovich and Kirby, 1987] Sirovich, L. and Kirby, M. (1987). Low dimensional procedure for the characterization of human faces. *Journal of Optical Society of America A*, 4.

[Sirovich et al., 1990b] Sirovich, L., Kirby, M., and Winter, M. N. (1990b). Eigenfunction approach to large scale transitional structures in jet flow. *Physics of Fluids A*, 2.

[Sirovich et al., 1990c] Sirovich, L., Rodriguez, J. D., and Knight, B. (1990c). Two boundary value problem for ginzburg-landau equation. *Physica D.*, 43.

[Sirovich and Zhou, 1994] Sirovich, L. and Zhou, X. (1994). Dynamical model of wall-bounded turbulence. *Physical Review Letters*, 72:340–343.

[Tarman, 2003] Tarman, I. H. (2003). A karhunen-loéve-based approach to numerical simulation of transition in Rayleigh-Benard convection. *Num. Heat Transfer B.*, 43.

[Tennekes and Lumley, 1972] Tennekes, H. and Lumley, J. L. (1972). *A first course in turbulence*. The MIT Press.

[Townsend, 1956] Townsend, A. A. (1956). *The Structure of Turbulent Shear Flow*. Cambridge University Press.

[Trefethen, 1997] Trefethen, L. N. (1997). Pseudospectra of linear operators. *SIAM Rev.*, 39:383.

[Trefethen, 2000] Trefethen, L. N. (2000). *Spectral Methods in MATLAB*. SIAM.

[Webber et al., 1997] Webber, G. A., Handler, R. A., and Sirovich, L. (1997). Karhunen Loéve decomposition of minimal channel flow. *Physics of Fluids*, 9:1054.

[Webber et al., 2002] Webber, G. A., Handler, R. A., and Sirovich, L. (2002). Energy dynamics in a turbulent channel flow using the Karhunen Loéve approach. *International Journal for Numerical Methods in Fluids*, 40:1381–1400.

APPENDIX A

Consider a continuous random filed $u(t)$ with

$$E\{u(t)\} = 0 \quad \text{and} \quad E\{|u(t)|^2\} < \infty \tag{A.1}$$

for $t \in [a, b]$, $u(t)$ is continuous in t for every $\epsilon > 0$, there is a $\delta > 0$ such that if $|h| \leq \delta$ then,

$$E\{|u(t) - u(t+h)|^2\} \leq \epsilon^2$$

Now define the covariance function by

$$R(t, s) = E\{u(t)\overline{u}(s)\} \tag{A.2}$$

$R(t, s)$ is continuous in t and s when $u(t)$ is continuous in t. The complex conjugate $\overline{(\cdot)}$ is included for generality. Suppose that there exists a deterministic function $\phi(t)$ in this random field, such that it has a structure typical of the ensemble of the random field. This suggests that the function $\phi(t)$ can be identified by maximizing the projection $u(t)$ an $\phi(t)$ which is given by

$$(u, \phi) \equiv \int_a^b u(t)\overline{\phi}(t)dt$$

in a Hilbert space, where $\phi(t)$ is a square integrable function. Since the value of (u, ϕ) must be independent of the magnitude of ϕ, the expression should be in the

form

$$(u,\phi)/(\phi,\phi)^{1/2}$$

If this idea is extended to the ensemble of $u(t)$, the expression must be maximized in some average sense. Then the problem arises that

$$E\{(u,\phi)\} = 0$$

by condition A.1. Hence the identification problem of the coherent structures (ϕ) must be posed as the maximization of the expression

$$E\{(u,\phi)\overline{(u,\phi)}\}/(\phi,\phi) = \lambda \geq 0 \tag{A.3}$$

Now, if $\phi(t)$ is continuous in t, then

$$\begin{aligned} E\{(u,\phi)\overline{(u,\phi)}\} \quad &= E\left\{\int_a^b u(t)\,\overline{\phi}(t)\,dt \int_a^b \overline{u}(s)\,\phi(s)\,ds\right\} \\ &= \int_a^b dt \int_a^b ds\,\phi(s)\,\overline{\phi}(t)\,E\,\{u(t)\overline{u}(s)\} \\ &= \int_a^b dt \int_a^b ds\,R(t,s)\,\phi(s)\,\overline{\phi}(t), \end{aligned}$$

so that (A.3) takes the form

$$\frac{\left(R(t,s)\,,\,\phi(t)\,\overline{\phi}(s)\right)}{(\phi(t),\phi(t))} = \lambda \geq 0$$

Suppose that $\phi(t)$ is the function which maximizes λ. Then any other function can be written as $\phi(t) + a\phi'(t)$, where a is a complex constant. Using the shorthand notation (ϕ for $\phi(t)$), λ can be written as

$$\frac{(R\,,\,\phi\,\overline{\phi}) + a(R\,,\,\phi\,\overline{\phi'}) + \overline{a}(R\,,\,\phi'\,\overline{\phi}) + a\,\overline{a}(R\,,\,\phi'\,\overline{\phi'})}{(\phi,\phi) + \overline{a}(\phi,\phi') + a(\phi',\phi) + a\,\overline{a}(\phi',\phi')} = \lambda$$

Since the maximum occurs when $a = 0$, the derivatives with respect to a and $\overline{a}$ at $a = 0$ must vanish. This results in

$$\left(R\,,\,\phi\,\overline{\phi'}\right) = \lambda(\phi'\,,\,\phi) \quad \text{and} \quad \left(R\,,\,\phi'\,\overline{\phi}\right) = \lambda(\phi\,,\,\phi') \tag{A.4}$$

Fro the definition A.2 of R ,

$$R(t,s) = \overline{R}(s,t) \tag{A.5}$$

it follows that

$$\begin{aligned}\left(R(t,s)\,,\,\phi'\,\overline{\phi}(s)\right) &= \left(\overline{R}(s,t)\,,\,\phi'(t)\,\overline{\phi}(s)\right)\\ &= \left(\overline{R}(t,s)\,,\,\overline{\phi}(t)\,\phi'(s)\right)\\ &= \left(R(t,s)\,,\,\phi(t)\,\overline{\phi'}(s)\right)^c\end{aligned}$$

where $(\cdot)^c$ denotes the complex conjugation operator, and

$$(\phi(t), \phi'(t)) = (\phi'(t), \phi(t))^c$$

so that the two equations in (A.4) are equivalent. If we take the equation for ϕ, i.e.,

$$\left(R\,,\,\phi\,\overline{\phi'}\right) = \lambda(\phi'\,,\,\phi)$$

which can be written as

$$\left(\left(R(t,s)\,,\,\overline{\phi}(s)\right) - \,\lambda\,\phi(t)\,,\,\phi'(t)\right) = 0$$

or

$$\left(R(t,s)\,,\,\overline{\phi}(s)\right) = \lambda\,\phi(t)$$

because ϕ' is an arbitrary function. Hence, the deterministic structure in the random field is the eigenfunction of the integral equation

$$\int_a^b R(t,s)\,\phi(s)\,ds = \lambda\,\phi(t) \tag{A.6}$$

with the covariance function $R(t,s)$ as the kernel.

The function $R(t,s)$ regarded as a kernel is continuous in both variables , hermitian (see cond (A.5)), non-negative and square integrable. Consequently, the solutions to (A.6) has some advantegous properties, discussed by the fundamental theorems for symmetric equations. Furthermore, since the integral in (A.6) is over a finite interval, Mercer's theorem applies as well. Thus the eigensolutions have the following properties.

1. There are not one, but a discrete set of solutions to (A.6), which can be written as

$$\int_a^b R(t,s)\,\phi^{(n)}(s)\,ds = \lambda^{(n)}\,\phi^{(n)}(t) \qquad n = 1, 2, \ldots$$

2. This set can be chosen such a way that $\phi^{(n)}$ are orthonormal, i.e.

$$\int_a^b \phi^{(n)}(s)\,\overline{\phi^{(m)}}(s)\,ds = \delta_{nm}$$

3. The eigenfunctions form a complete set of functions $\left\{\phi^{(n)}\right\}$, so that the random field may be expanded in them, such that

$$u(t) = \sum_n a_n\,\phi^{(n)}(t)$$

where

$$a_n = \left(u\,,\,\phi^{(n)}\right) = \int_a^b u(t)\,\overline{\phi^{(n)}}(t)\,dt$$

and the series converges in the mean square.

4. The random coefficients in item 3 are statistically uncorrelated, i.e.

$$\begin{aligned} E\left\{\left(u\,\phi^{(n)}\right)\left(u,\,\phi^{(n)}\right)^{c}\right\} &= \left(R(t,s)\,,\,\phi^{(n)}(t)\,\overline{\phi^{(m)}}(t)\right) \\ &= \lambda^{(m)}\left(\phi^{(m)}(t)\,,\phi^{(n)}(t)\right) \\ &= \lambda^{(m)}\delta_{mn} \end{aligned}$$

5. $R(t,s)$ may be decomposed into a double series in $\phi^{(n)}$ as follows,

$$\begin{aligned} R(t,s) &= E\left\{u(t)\,,\,\overline{u}(s)\right\} \\ &= \sum_n \sum_m \phi^{(n)}(t)\,\overline{\phi^{(m)}}(s)\,E\{a_n\,\overline{a}_m\} \\ &= \sum_n \sum_m \lambda^{(m)}\,\delta_{nm}\,\phi^{(n)}(t)\,\overline{\phi^{(m)}}(s) \\ &= \sum_m \lambda^{(m)}\,\phi^{(m)}(t)\,\overline{\phi^{(m)}}(s) \end{aligned}$$

and the series converges uniformly and absolutely.

6. The eigenvalues $\lambda^{(n)}$ are real, non-negative and their sum is finite, i.e.

$$\lambda^{(n)} \geq 0$$

$$\begin{aligned} E\{(u\,,\,u)\} &= \int_a^b R(t,t)\,dt \\ &= \sum_m \lambda^{(m)} \int_a^b \phi^{(m)}(t)\,\overline{\phi^{(m)}}(t)\,dt \\ &= \sum_m \lambda^{(m)} < \infty \end{aligned}$$

by the relation A.1

So the search for the deterministic function $\phi(t)$ which maximizes the mean square of $(u\,,\,\phi)$ in some average sense results in a discrete set of solutions. These set of eigenfunctions are orthogonal to each other, so each eigenfunction encompasses aspects of the function u, which cannot be accomodated in the other eigenfunctions. The decomposition of the random field into these deterministic structures is optimal in the sense that each structure holds a large portion of the energy of the field as it possibly can. This is a consequence of the fact that each structure is found by extremization of the corresponding eigenvalue λ which represents the fraction of the total energy that the structure holds.

There is one case that the solution to the integral equation (A.6) takes a simple form. This is the case where t is a homogenous coordinate. Then $R(t,s)$ depends on the distance between the two coordinate points, i.e.

$$R(t\,,\,s) = R(s-t)$$

Morover if the kernel is L-periodic in s and t, i.e.

$$R(t\,,\,s) = R(t+mL\,,\,s+nL) \quad \forall n,m \in \mathbf{I}$$

where $L = b - a$, then (A.6) becomes

$$\int_a^b R(s-t)\,\phi(s)\,ds = \lambda\,\phi(t)$$

Now suppose that,

$$\phi(s) = e^{(i\,\frac{2\pi}{L}\,k\,s)} \quad k \in \mathbf{I} \tag{A.7}$$

then

$$\int_a^b R(s-t)\,e^{(i\,\frac{2\pi}{L}\,k\,s)}\,ds = \lambda(k)$$

let $r = s - t$ than

$$\int_{-L/2}^{L/2} R(r)\,e^{(i\,\frac{2\pi}{L}\,k\,r)}\,dr = \lambda(k)$$

since the kernel is Hermitian, this reduces to

$$2 \int_{-L/2}^{L/2} R(r)\, \cos\left(\frac{2\pi}{L}\, k\, r\right) dr = \lambda(k) \tag{A.8}$$

This is equivalent to saying that in the homogenous direction, the sinusoids (A.7) are suitable solutions to (A.6) and the eigenvalues are given by (A.8)

APPENDIX B

In order to construct spectral approximation to Orr-Sommerfeld differential eigenvalue problem, let $\{v_j\}$ be the vector of values of v sampled at the Chebyshev-Lobatto points, $x_j = \cos(\pi j/N)$,$j = 1, \ldots, N-1$. The polynomial interpolant $p(x)$, satisfying the boundary conditions can be constructed as follows

- Let p be the unique polynomial of degree $\leq N+2$ with $p(\pm 1) = p_x(\pm 1) = 0$ and $p(x_j) = v_j$ for $j = 1, \ldots, N-1$

- Then the high derivatives can be computed by differentiating $p(x)$

If we set

$$p(x) = (1 - x^2)q(x),$$

Then, a polynomial q of degree $\leq N$ with $q(\pm 1) = 0$ corresponds to a polynomial p of degree $\leq N+2$ with $q(\pm 1) = q_x(\pm 1) = 0$.

Now we can carry out the differentiation as follows

- Let q be the unique polynomial of degree $\leq N$ with $q(\pm 1) = 0$ and $q(x_j) = v_j/(1 - x^2)$ for $j = 1, \ldots, N-1$

- The derivatives are then discretized to yield:

$$p_{xxxx} \Longrightarrow D4 \equiv \left[\text{diag}(1-x_j^2)\tilde{D}_N^{(4)} - 8\text{diag}(x_j\tilde{D}_N^{(3)} - 12\tilde{D}_N^{(2)}\right] \times \text{diag}\left(\frac{1}{1-x_j^2}\right)$$

$$p_{xxx} \Longrightarrow D3 \equiv \left[\text{diag}(1-x_j^2)\tilde{D}_N^{(3)} - 6\text{diag}(x_j\tilde{D}_N^{(2)} - 6\tilde{D}_N^{(2)}\right] \times \text{diag}\left(\frac{1}{1-x_j^2}\right)$$

$$p_{xx} \Longrightarrow D2 \equiv \tilde{D}^{(2)}$$

where $\tilde{D}_N^{()}$ are the higher-order Chebyshev differentiation matrices obtained by taking the indicated powers of D_N and stripping away the first and last rows and columns in order to satisfy th boundary conditions [Trefethen, 2000].

```
% orr.m - eigenvalues and eigenmodes of Orr-Sommerfeld operator

  R = 10000; a = 1; b = 0; ab = a^2 + b^2; N = 120; clf

    % 2nd- and 4th-order differentiation matrices:
    [D,x] = cheb(N); D2 = D^2; D2 = D2(2:N,2:N);
    S = diag([0; 1 ./(1-x(2:N).^2); 0]);
    D4 = (diag(1-x.^2)*D^4 - 8*diag(x)*D^3 - 12*D^2)*S;
    D4 = D4(2:N,2:N);

    % Orr-Sommerfeld operators A,B and generalized eigenvalues:
    I = eye(N-1);
    A = -(D4-2*ab*D2+(ab^2)*I)/R + 2i*a*I + 1i*a*diag(1-x(2:N).^2)*(D2-ab*I);
    B = 1i*(D2-ab*I);
    [eigm,eigv] = eig(A,B); ee = diag(eigv);
    index = find((imag(ee)==max(imag(ee))));
    vz = [0; eigm(:,index); 0];

    % Vertical vorticity component
    for k = 1:N-1
        LHS = B/R + ((a*diag(1-x(2:N).^2)-ee(k)*I));
        RHS = 2*b*diag(x(2:N))*eigm(:,k);
        nuk = LHS \ RHS; nu(:,k) = [0; nuk; 0];
    end
    nuz = nu(:,index);

    % Horizontal velocity components
    uz = (-1i*b*nuz + 1i*a*D*vz)/ab;
    wz = (1i*a*nuz + 1i*b*D*vz)/ab;
```